

What are C and h ? : Inequalities for the analysis and design of finite element methods

Isaac Harari and Thomas J.R. Hughes

Division of Applied Mechanics, Stanford University, Stanford, CA 94305-4040, USA

Received 20 March 1991

Increasing mathematical analysis of finite element methods is motivating the inclusion of mesh-dependent terms in new classes of methods for a variety of applications. Several inequalities of functional analysis are often employed in convergence proofs. In the following, Poincaré–Friedrichs inequalities, inverse estimates and least-squares bounds are characterized as tools for the error analysis and practical design of finite element methods with terms that depend on the mesh parameter. Sharp estimates of the constants of these inequalities are provided, and precise definitions of mesh size that arise naturally in the context of different problems in terms of element geometry are derived.

1. Introduction

The process of designing finite element methods has become increasingly dependent in recent years on understanding the mathematical framework underlying this methodology. This is evident from the advent of a profusion of new classes of methods which are founded on the basis of error analysis [1–9]. In such cases, additional quantities are introduced into the formulation in order to demonstrate convergence of numerical solutions to the exact solution, usually at optimal or quasi-optimal rates. By endowing the method in this manner with a sound mathematical foundation, its performance on general configurations is guaranteed and specific attributes are improved. In many instances this procedure enhances stability properties while maintaining higher-order accuracy.

Such ideas were developed by Hughes and Brooks for problems of convective transport [6], and originally referred to as ‘streamline-upwind/Petrov–Galerkin’ (SUPG, also called ‘streamline-diffusion’ and ‘anisotropic balancing diffusion’). These methods were later extended to advective-diffusive systems [10, 11], applied to Stokes [12], and compressible and incompressible flows [9, 13–15], and have since undergone extensive refinement and mathematical analysis (for a review see [16; 17, pp. 181–188, 199–204, 259–268] and references therein).

In a relatively recent development, the concept of ‘Galerkin/least-squares’ has arisen as a generalization of these ideas. This methodology is obtained by appending terms in *least-squares form* to the standard Galerkin formulation. The added terms contain *residuals of the Euler–Lagrange equations* of the boundary-value problem usually evaluated over element interiors, thereby preserving the *consistency* inherent in the Galerkin method (an important ingredient in obtaining improved convergence rates with higher-order interpolation) as well as respecting regularity requirements on the functions employed. The notion of Galerkin/least-squares crystallized in [7] and in the application of ideas of this sort to abstract mixed problems by Franca and Hughes (see [4] and references therein) and their colleagues, and was the key to recognizing these techniques as part of a general framework.

In fluid mechanics, Galerkin/least-squares methods are identical to SUPG for hyperbolic cases, but the analysis in the presence of diffusion is simpler [7]. For mixed problems, critical stability conditions governing well-posedness are violated in the Galerkin framework by many practically convenient interpolations. Under the Galerkin/least-squares umbrella, general combinations of interpolations (including equal-order ones) become convergent, either by *circumventing* the stability conditions in the case of Stokes [18], compressible and incompressible elasticity [19], Reissner–Mindlin plate [20] and contact problems [21] (in which the constraints are on the boundaries), or by *satisfying* these conditions in the application of variational principles (such as Hellinger–Reissner formulations) to compressible and incompressible elasticity [22], and structural models (see [4] and references therein). In a similar application, mixed variational principles of linear elasticity with independent rotation fields are modified to engender displacement-type formulations that converge for all combinations of interpolations [5, 23]. These formulations lead to membrane elements with drilling (in-plane rotational) degrees of freedom in the two-dimensional case, which may be employed to facilitate the analysis of shells. The Galerkin/least-squares technology has been exploited to relax wave-resolution requirements in problems of time-harmonic acoustics [24, 25]. Galerkin/least-squares methods have also been implemented as a crucial stabilizing ingredient in space-time finite element methods both for first-order [7, 11] and second-order hyperbolic equations [8].

Other alternatives to the basic Galerkin formulation may be constructed without upsetting consistency. Douglas and Wang modified the Galerkin/least-squares method for Stokes flow presented in [18] by altering the *weighting* of the additional terms [1]. This nonsymmetric formulation, which is stable under more lenient conditions than its Galerkin/least-squares counterpart, was later extended to advection-diffusion problems [3]. A modification to the treatment of the jump terms in [18] is presented in [26]. Franca and Dutra do Carmo introduced a method they called ‘Galerkin/gradient least-squares’ in which the least-squares terms contain residuals of the *gradient* of the governing differential equation [2]. This method is intended for modeling complex boundary layer phenomena, such as arise in the analysis of thin structures, and thus far was successfully applied to scalar singular diffusion problems.

In most of the aforementioned applications the added terms depend on the mesh parameter. The proper dependence of these quantities on the order of the mesh parameter and the magnitude of scaling coefficients is dictated in general by the error analysis and often made precise by examining model problems. Convergence proofs frequently make use of well-known inequalities of functional analysis. For the purpose of analysis it is sufficient to know that these inequalities hold for constants that are positive, and for general-purpose definitions of the mesh parameter (e.g., the length of the longest element side in the mesh) for regular elements (i.e., aspect ratios and distortion are limited) on quasi-uniform meshes (in which elements are of essentially the same size). With reference to this terminology see, e.g., [17, pp. 45, 84–85, 141]. (These restrictions on the mesh are frequently violated in the computation of solutions to engineering problems. For example, in the finite element analysis of compressible viscous flows, elements with aspect ratios as high as order 1000 are commonly employed in the discretization of boundary layers [13, 27], ratios of element sizes in a mesh can be of the same order [28] and significant element distortion may be evident [29]. Similar departures from the ideal conditions of employing quasi-uniform meshes of regular elements are also evident in large deformation and impact problems of finite elasticity [30, pp. 79–91; 31, 32]). In contrast to the perspective of mathematical analysis, when constructing methods for practical implementation designers need to be concerned with precise contextual definitions of the element size and sharp estimation of the constants to determine the coefficients of the least-squares terms. Indeed, there is ongoing research on the appropriate treatment of this

crucial aspect of method design for some formulations that contain terms which depend on the mesh parameter (see, e.g., [3]). One-dimensional model problems may provide detailed information on these quantities in a limited setting, but such models are not always readily available, and natural generalizations of the one-dimensional definition of the mesh parameter (as the element length) are not necessarily straightforward.

In the following we address these issues by characterizing in detail the relevant inequalities of functional analysis, thereby providing tools for the mathematical analysis of finite element methods, as well as their design in practice. Various techniques employed in estimating the coefficients are demonstrated, and those quantities are computed for many cases. In Section 2 constants are evaluated for Poincaré–Friedrichs inequalities in which lower derivatives of functions are bounded by higher derivatives. To our knowledge the estimate presented for the general case therein is sharper than hitherto known, and the specialization to annular regions not performed elsewhere. This result is also extended to Neumann problems. Inverse estimates for a variety of applications are presented in Section 3. In contrast to Poincaré–Friedrichs inequalities, inverse estimates bound higher derivatives by lower derivatives, and hold only for finite-dimensional function spaces. These inequalities emanate from element-level eigenvalue problems and are therefore properly stated over individual elements or the union thereof. (Similar eigenvalue problems are used to estimate critical time steps for stability in transient finite element analysis, as presented in [33, pp. 513–523, and references therein; 34].) Results based on inverse estimates may therefore be applied without concern for quasi-uniformity of meshes. In addition to sharp estimates of the constants for these inequalities we also obtain concrete definitions of the size of different elements that arise naturally in the context of various problems. These precise definitions are based on element geometry in terms of such quantities as the coordinates of the vertex nodes, the length of the element sides, the element area and the radius of the circumscribing circle. (Similar extensions of critical time-step estimation to one-point quadrature elements with arbitrary geometries were performed in [35], although many of the results presented therein approximate the geometry by trial and error.) Since aspect ratios and distortion are accounted for, these results are not restricted to regular elements. In Section 4 we present ‘least-squares bounds’ which are a recent extension of inverse estimates that arises naturally in the context of Galerkin/least-squares methods. The preceding remarks on the validity of results based on properly stated inverse estimates beyond configurations employing regular elements on quasi-uniform meshes apply to these inequalities as well. Furthermore, least-squares bounds directly exhibit the beneficial influence of least-squares quantities in controlling destabilizing terms. For problems of time-harmonic acoustics, where least-squares bounds were introduced and employed to demonstrate convergence, inverse estimates are apparently not sufficiently strong for this purpose. We conjecture that these inequalities may lead to improved or conceptually simpler analysis in other applications as well. Closing remarks are presented in Section 5. In Appendix A several well-known inequalities are presented, and results for inverse estimates from Section 3 are summarized in Appendix B.

For generality, functions in the following may be scalar, vector or tensor valued as appropriate, as well as either real valued or complex valued, unless specified. Functions are defined over the open bounded domain $\Omega \subset \mathbb{R}^d$, where d is the number of space dimensions. Let $L_2(\Omega)$ denote the space of square-integrable functions on Ω , and $H^1(\Omega)$ denote the space of functions in $L_2(\Omega)$ with generalized derivatives also in $L_2(\Omega)$. The subset of $H^1(\Omega)$ whose members vanish on the boundaries is $H_0^1(\Omega)$. The scalar field K represents either \mathbb{R} or \mathbb{C} . Let $(\cdot, \cdot) : \mathcal{V} \times \mathcal{V} \rightarrow K$ be the $L_2(\Omega)$ inner product on the vector space \mathcal{V} (with the first argument conjugated, if need be). The norm induced by this inner product is $\|\cdot\| : \mathcal{V} \rightarrow \mathbb{R}$. Subscripts on inner products and norms denote domains of integration other than Ω .

2. Poincaré–Friedrichs inequalities

Poincaré–Friedrichs inequalities typically bound functions in terms of their derivatives scaled by a domain-dependent coefficient. See, e.g., [36, p. 94] and references therein, for a function-analytical overview of inequalities of this type. Versions of Poincaré–Friedrichs inequalities have numerous applications in the analysis of finite element methods [22; 25; 37, pp. 3, 25–26; 38, p. 69].

2.1. Estimation of the constant

The constant of the inequality, $C(\Omega)$, depends only on the domain of the function. Its estimate is obtained directly from the proof of the inequality.

One dimension: This version of the inequality ($d = 1$) is derived in [38, p. 42], and is reviewed here along the lines of [39, pp. 161–162], improving the estimate of the constant by a factor of two. For functions w possessing square-integrable derivatives, defined on the open interval $\Omega =]0, L[$, with the boundary condition $w(0) = 0$,

$$\frac{L^2}{2} \|\nabla w\|^2 \geq \|w\|^2. \quad (1)$$

The proof of this statement begins with the fundamental theorem of integral calculus, namely

$$w(x) = \int_0^x \frac{dw}{dx}(\xi) d\xi. \quad (2)$$

Squaring both sides

$$\begin{aligned} |w(x)|^2 &= \left| \int_0^x 1 \frac{dw}{dx} d\xi \right|^2 \\ &\leq \int_0^x 1^2 d\xi \int_0^x \left| \frac{dw}{dx} \right|^2 d\xi \\ &\leq x \int_0^L \left| \frac{dw}{dx} \right|^2 dx \\ &= x \|\nabla w\|^2, \end{aligned} \quad (3)$$

where line two of (3) was obtained by applying the Schwarz inequality, (A.1) in Appendix A.

$$\|w\|^2 = \int_0^L |w(x)|^2 dx \leq \int_0^L x dx \|\nabla w\|^2 = \frac{L^2}{2} \|\nabla w\|^2. \quad (4)$$

General case: There exists a positive constant $C(\Omega)$ such that

$$C(\Omega) \|\nabla w\|^2 \geq \|w\|^2 \quad \forall w \in H_0^1(\Omega). \quad (5)$$

A proof for this multi-dimensional case is presented in [40, pp. 9, 10]. The constant of the inequality is corrected in [39, pp. 164, 165], and is further improved in the following. In keeping with the notation of [40], $\mathcal{D}(\Omega)$ denotes the space of infinitely-differentiable functions

with compact support in Ω . In evaluating the constant we will refer to the length of the sides of a right-angle parallelepiped that contains the domain (which is bounded), namely $\Omega \subset [a_1, b_1] \times \cdots \times [a_d, b_d]$. For functions $w \in \mathcal{D}(\Omega)$

$$w(x) = \int_{a_i}^{x_i} \frac{\partial w}{\partial x_i} (x_1, \dots, x_{i-1}, \xi, x_{i+1}, \dots, x_d) d\xi, \quad (6)$$

$$|w(x)|^2 \leq \int_{a_i}^{x_i} 1^2 d\xi \int_{a_i}^{x_i} \left| \frac{\partial w}{\partial x_i} \right|^2 d\xi \leq (x_i - a_i) \int_{a_i}^{b_i} \left| \frac{\partial w}{\partial x_i} \right|^2 dx, \quad (7)$$

$$\begin{aligned} \|w\|^2 &= \int_{a_1}^{b_1} \cdots \int_{a_d}^{b_d} |w(x)|^2 d\Omega \\ &\leq \int_{a_i}^{b_i} (x_i - a_i) dx_i \int_{a_1}^{b_1} \cdots \int_{a_d}^{b_d} \left| \frac{\partial w}{\partial x_i} \right|^2 d\Omega \\ &= \frac{(b_i - a_i)^2}{2} \left\| \frac{\partial w}{\partial x_i} \right\|^2 \\ &\leq \frac{(b_i - a_i)^2}{2} \|\nabla w\|^2, \end{aligned} \quad (8)$$

and since this inequality holds for any $1 \leq i \leq d$,

$$\|w\|^2 \leq \frac{1}{2} \min_{1 \leq i \leq d} (b_i - a_i)^2 \|\nabla w\|^2. \quad (9)$$

Alternatively, the third line of (8) may be summed over $1 \leq i \leq d$, yielding

$$\begin{aligned} d\|w\|^2 &\leq \frac{1}{2} \sum_{i=1}^d (b_i - a_i)^2 \left\| \frac{\partial w}{\partial x_i} \right\|^2 \\ &\leq \frac{1}{2} \max_{1 \leq i \leq d} (b_i - a_i)^2 \|\nabla w\|^2. \end{aligned} \quad (10)$$

Applying the density of $\mathcal{D}(\Omega)$ in $H_0^1(\Omega)$ verifies (5) with

$$C(\Omega) = \frac{1}{2} \min \left\{ \min_{1 \leq i \leq d} (b_i - a_i)^2, \frac{1}{d} \max_{1 \leq i \leq d} (b_i - a_i)^2 \right\}. \quad (11)$$

For problems in slender and thin regions the first part of the estimate is sharper, whereas the second part is more suitable for domains that approximate balls. Overall we are not aware of as sharp an estimate previously known for arbitrary multi-dimensional domains.

Annular regions: The estimate of the constant (11) can be improved for specific regions. Consider, for example, domains that are conveniently bounded between concentric spheres, such as arise in the solution of problems in unbounded domains by the DtN method [41], i.e., $\Omega \subset \{x \in \mathbb{R}^d \mid a < |x| < R\}$. The limiting case in which $a \rightarrow 0$ is also easily accommodated in the following.

For $d=2$ it is convenient to work in polar coordinates (r, θ) , where $d\Omega = r dr d\theta$. For functions $w \in \mathcal{D}(\Omega)$

$$w(r, \theta) = \int_a^r \frac{\partial w}{\partial r}(\rho, \theta) d\rho, \quad (12)$$

$$|w(r, \theta)|^2 \leq \int_a^r \frac{1}{\rho} d\rho \int_a^r \left| \frac{\partial w}{\partial r} \right|^2 \rho d\rho \leq \ln \frac{r}{a} \int_a^r \left| \frac{\partial w}{\partial r} \right|^2 r dr, \quad (13)$$

$$\begin{aligned} \|w\|^2 &= \int_a^R \int_0^{2\pi} |w(r, \theta)|^2 r dr d\theta \\ &\leq \int_a^R r \ln \frac{r}{a} dr \int_\Omega \left| \frac{\partial w}{\partial r} \right|^2 d\Omega \\ &= \left(\frac{R^2}{2} \ln \frac{R}{a} - \frac{R^2 - a^2}{4} \right) \left\| \frac{\partial w}{\partial r} \right\|^2 \\ &\leq \left(\frac{R^2}{2} \ln \frac{R}{a} - \frac{R^2 - a^2}{4} \right) \|\nabla w\|^2. \end{aligned} \quad (14)$$

Similarly

$$-w(r, \theta) = \int_r^R \frac{\partial w}{\partial r}(\rho, \theta) d\rho, \quad (15)$$

$$|w(r, \theta)|^2 \leq \ln \frac{R}{r} \int_r^R \left| \frac{\partial w}{\partial r} \right|^2 r dr, \quad (16)$$

$$\|w\|^2 \leq \left(\frac{R^2 - a^2}{4} - \frac{a^2}{2} \ln \frac{R}{a} \right) \|\nabla w\|^2. \quad (17)$$

To determine which of the coefficients is lower we note that

$$\begin{aligned} \ln x &= 2 \sum_{n=0}^{\infty} \frac{1}{2n+1} \left(\frac{x-1}{x+1} \right)^{2n+1} \quad \forall x > 0 \\ &> 2 \frac{x-1}{x+1} \quad \forall x > 1 \\ &\geq \frac{x^2 - 1}{x^2 + 1}, \end{aligned} \quad (18)$$

where the last line follows from (A.4) in Appendix A and is easily verified. Consequently

$$\ln \frac{R}{a} \geq \frac{R^2 - a^2}{R^2 + a^2} \quad \forall R > a, \quad (19)$$

and so, for this case

$$\begin{aligned} \min \left\{ \frac{R^2}{2} \ln \frac{R}{a} - \frac{R^2 - a^2}{4}, \frac{R^2 - a^2}{4} - \frac{a^2}{2} \ln \frac{R}{a} \right\} &= \frac{R^2 - a^2}{4} - \frac{a^2}{2} \ln \frac{R}{a} \\ &\rightarrow \frac{R^2}{4} \quad \text{as } a \rightarrow 0. \end{aligned} \quad (20)$$

In the three-dimensional case we work in spherical coordinates (r, θ, φ) , where $d\Omega = r^2 \sin \varphi dr d\theta d\varphi$. Again, for functions $w \in \mathcal{D}(\Omega)$,

$$w(r, \theta, \varphi) = \int_a^r \frac{\partial w}{\partial r}(\rho, \theta, \varphi) d\rho, \quad (21)$$

$$|w(r, \theta, \varphi)|^2 \leq \int_a^r \frac{1}{\rho^2} d\rho \int_a^r \left| \frac{\partial w}{\partial r} \right|^2 \rho^2 d\rho \leq \left(\frac{1}{a} - \frac{1}{r} \right) \int_a^r \left| \frac{\partial w}{\partial r} \right|^2 r^2 dr, \quad (22)$$

$$\begin{aligned} \|w\|^2 &= \int_{r=a}^R \int_{\theta=0}^{2\pi} \int_{\varphi=0}^{\pi} |w(r, \theta, \varphi)|^2 r^2 \sin \varphi dr d\theta d\varphi \\ &\leq \int_a^R r^2 \left(\frac{1}{a} - \frac{1}{r} \right) dr \int_{\Omega} \left| \frac{\partial w}{\partial r} \right|^2 d\Omega \\ &= \frac{(R-a)^2(2R+a)}{6a} \left\| \frac{\partial w}{\partial r} \right\|^2 \\ &\leq \frac{(R-a)^2(2R+a)}{6a} \|\nabla w\|^2. \end{aligned} \quad (23)$$

Likewise

$$-w(r, \theta, \varphi) = \int_r^R \frac{\partial w}{\partial r}(\rho, \theta, \varphi) d\rho, \quad (24)$$

$$|w(r, \theta, \varphi)|^2 \leq \left(\frac{1}{r} - \frac{1}{R} \right) \int_a^R \left| \frac{\partial w}{\partial r} \right|^2 r^2 dr, \quad (25)$$

$$\|w\|^2 \leq \frac{(R-a)^2(R+2a)}{6R} \|\nabla w\|^2. \quad (26)$$

In this case

$$\begin{aligned} \frac{(R-a)^2}{6} \min\{2R+a, R+2a\} &= \frac{(R-a)^2(R+2a)}{6R} \quad \forall R > a \\ &\rightarrow \frac{R^2}{6} \quad \text{as } a \rightarrow 0. \end{aligned} \quad (27)$$

For both multi-dimensional cases, applying the density of $\mathcal{D}(\Omega)$ in $H_0^1(\Omega)$ verifies (5) with

$$\begin{aligned} C(\Omega) &= \begin{cases} \frac{R^2 - a^2}{4} - \frac{a^2}{2} \ln \frac{R}{a}, & d=2 \\ \frac{(R-a)^2(R+2a)}{6R}, & d=3 \end{cases} \\ &\rightarrow \frac{R^2}{2d} \quad \text{as } a \rightarrow 0, \end{aligned} \quad (28)$$

which is an improvement of a factor of four over the constant for the general case (11) for domains that approximate balls. Such specializations of Poincaré–Friedrichs inequalities to annular regions leading to sharper estimates of the constant have not been presented elsewhere, inasmuch as the authors are aware.

REMARK. Similar improvements are possible for other special cases of interest such as domains conveniently bounded by ellipsoids or cylinders.

2.2. Neumann problems

Poincaré–Friedrichs inequalities are most frequently employed for Dirichlet problems. For problems with only Neumann-type boundary conditions boundary terms must be included in the inequalities and carefully characterized. This is immediately evident from the generalization of the one-dimensional case presented in [25], for functions w defined on the open interval $\Omega =]0, L[$,

$$\begin{aligned} \frac{L^2}{2} \|\nabla w\|^2 &\geq \|w(x) - w(L)\|^2 \quad \forall w \in H^1(\Omega) \\ &\geq \frac{1}{1+\epsilon} \|w\|^2 - \frac{L}{\epsilon} |w(L)|^2 \quad \forall \epsilon > 0, \end{aligned} \quad (29)$$

where the first line above follows from the one-dimensional Poincaré–Friedrichs inequality (1) (which is unchanged when the homogeneous Dirichlet boundary condition at $x = 0$ is replaced with $w(L) = 0$), and in the second line we made use of the left-hand inequality of (A.4) in Appendix A. For the time-harmonic acoustic problems examined in [25], the value of $\epsilon = 2/(|k|L)$ was chosen so that

$$\|w\|^2 \leq \frac{(2 + |k|L)L}{2|k|} (\|\nabla w\|^2 + |k| |w(L)|^2). \quad (30)$$

The wave number k has dimensions of inverse length and $k^2 \in \mathbb{R}$.

Similar results may be obtained in multi-dimensional cases for functions $w \in H^1(\Omega)$, where Ω has an external boundary $\partial\mathcal{B}_R$, which is a sphere of radius R centered at the origin, and, possibly, an internal boundary that circumscribes a sphere of radius a centered at the origin (i.e., a may be zero). In two dimensions, cf. (15),

$$w(R, \theta) - w(r, \theta) = \int_r^R \frac{\partial w}{\partial r}(\rho, \theta) d\rho, \quad (31)$$

$$\begin{aligned} \left(\frac{R^2 - a^2}{4} - \frac{a^2}{2} \ln \frac{R}{a} \right) \|\nabla w\|^2 &\geq \|w(r, \theta) - w(R, \theta)\|^2 \\ &\geq \frac{1}{1+\epsilon} \|w\|^2 - \frac{R^2 - a^2}{2\epsilon R} \int_0^{2\pi} |w(R, \theta)|^2 R d\theta, \end{aligned} \quad (32)$$

and in three dimensions, cf. (24),

$$w(R, \theta, \varphi) - w(r, \theta, \varphi) = \int_r^R \frac{\partial w}{\partial r}(\rho, \theta, \varphi) d\rho, \quad (33)$$

$$\begin{aligned} \frac{(R-a)^2(R+2a)}{6R} \|\nabla w\|^2 &\geq \|w(r, \theta, \varphi) - w(R, \theta, \varphi)\|^2 \\ &\geq \frac{1}{1+\epsilon} \|w\|^2 \\ &\quad - \frac{R^3 - a^3}{3\epsilon R^2} \int_{\theta=0}^{2\pi} \int_{\varphi=0}^{\pi} |w(R, \theta, \varphi)|^2 R^2 \sin \varphi d\theta d\varphi. \end{aligned} \quad (34)$$

These inequalities may be combined for the case in which $a \rightarrow 0$ to yield a generalization of (3), namely

$$\|w\|^2 \leq \frac{(2 + |k|R)R}{2|k|d} (\|\nabla w\|^2 + |k| \|w\|_{\partial\mathcal{B}_R}^2) \quad (35)$$

by selecting $\epsilon = 2/(|k|R)$.

3. Inverse estimates

Inverse estimates are inequalities that are valid for finite-dimensional function spaces \mathcal{V}^h , subsets of the space of admissible functions \mathcal{V} , where h denotes the mesh parameter. The label ‘inverse’ is used in relation to Poincaré–Friedrichs inequalities, since in this case lower derivatives in linear differential operators bound higher derivatives. Results of this kind are discussed in [17, pp. 141–145; 42, pp. 140–146]. Inverse estimates have been used extensively in the analysis of finite element methods [7, 11, 20]. We restrict our attention in the following to finite element functions, i.e., piecewise polynomials, that are associated with Lagrange-type interpolation (see, e.g., [33, pp. 126–131, 164–170]). As previously stated, inverse estimates emanate from element-level inequalities. The class of polynomials of degree no greater than l on the element interior Ω^e is denoted $\mathcal{P}^l(\Omega^e)$.

For a given boundary-value problem, or pair of operators, the constant of the inverse estimate $C_l \geq 0$ is independent of h and depends only on the degree of interpolation l . For any specific case C_l increases monotonically with l , and in general $C_l \rightarrow \infty$ as $l \rightarrow \infty$. A variety of techniques for estimation of constants is presented in the following. The subsequent calculations are valid for elements with a constant Jacobian, i.e., higher-order elements have straight edges and mid-nodes are placed appropriately. For more general cases, these results may be thought of as estimates in the parent domain (with suitable values for h) and isoparametric mappings may be employed to transform the estimates to physical space.

In the following, inverse estimates for problems of advection-diffusion, incompressible elasticity (and Stokes flow) and shear-deformable plates are investigated. These results are summarized in Appendix B.

3.1. Advection-diffusion

The steady-state scalar advection-diffusion problem gives rise to one of the simpler forms of the inverse estimate, which will be used to demonstrate alternative approaches to presenting the inequality and determining the constant. Examples of the application of inverse estimates to advection-diffusion problems are found in [3, 7, 10, 11]. In this inequality the gradient bounds Laplacian

$$(h^e)^2 \|\Delta w^h\|_{\Omega^e}^2 \leq C_l \|\nabla w^h\|_{\Omega^e}^2 \quad \forall w^h \in \mathcal{V}^h, \quad (36)$$

where h^e is the element size, to be defined specifically for each element type so that C_l depends only on the interpolation employed. Element-level inequalities may be combined over a mesh containing n_{el} elements employing identical interpolation,

$$\sum_{e=1}^{n_{el}} (h^e)^2 \|\Delta w^h\|_{\Omega^e}^2 \leq C_l \|\nabla w^h\|^2 \quad \forall w^h \in \mathcal{V}^h. \quad (37)$$

Defining the mesh parameter as $h = \min_{1 \leq e \leq n_{el}} h^e$ leads to a global statement of the inverse estimate that is often presented,

$$h^2 \sum_{e=1}^{n_{el}} \|\Delta w^h\|_{\Omega^e}^2 \leq C_l \|\nabla w^h\|^2 \quad \forall w^h \in \mathcal{V}^h, \quad (38)$$

but we prefer (36) since it emphasizes the element-level nature of the inequality.

In simple cases the constant may be determined by expressing the restriction of finite element functions to the element domain as polynomials with unknown coefficients and substituting directly into the local version of the inverse estimate (36). For higher-order elements the process of determining the constant and the appropriate element size becomes quite difficult. To simplify matters, the number of independent coefficients may be reduced by considering only functions $\bar{w}^h \in \mathcal{P}^l(\Omega^e)$ such that

$$\left. \begin{aligned} \|\nabla \bar{w}^h\|_{\Omega^e} &\leq \|\nabla w^h\|_{\Omega^e} \\ \Delta \bar{w}^h &= \Delta w^h \end{aligned} \right\} \quad \forall w^h \in \mathcal{P}^l(\Omega^e). \quad (39)$$

The element-level problem can be characterized variationally by the Rayleigh quotient

$$\lambda^h = \max_{w^h \in \mathcal{P}^l(\Omega^e)} \frac{\|\Delta w^h\|_{\Omega^e}^2}{\|\nabla w^h\|_{\Omega^e}^2}. \quad (40)$$

Then

$$C_l = \lambda^h (h^e)^2, \quad (41)$$

which is independent of h . The Rayleigh quotient may be evaluated directly as the maximum eigenvalue of the associated problem: Find $\{\lambda^h, v^h\}$, $v^h \in \mathcal{P}^l(\Omega^e)$ such that

$$(\Delta w^h, \Delta v^h)_{\Omega^e} - \lambda^h (\nabla w^h, \nabla v^h)_{\Omega^e} = 0 \quad \forall w^h \in \mathcal{P}^l(\Omega^e), \quad (42)$$

where the matrices involved are computed by standard finite element methodology. The variational characterization of the problem may also be simplified by considering functions \bar{w}^h as in (39) instead of w^h .

One dimension: In this case the definition of the element size h^e as the element length is straightforward, and the evaluation of the constant is relatively simple. For convenience we consider the element domain to be the open interval $\Omega^e =]-h^e/2, h^e/2[$ (Fig. 1), and we examine finite element functions and their derivatives restricted to that domain. For linear elements ($l = 1$) the constant is trivial since

$$w^h|_{\Omega^e} = a_0 + a_1 x. \quad (43)$$

In this case $\Delta w^h|_{\Omega^e} = 0$ and hence $C_l = 0$.

For quadratic elements ($l = 2$) we employ direct substitution

$$w^h|_{\Omega^e} = a_0 + a_1 x + a_2 x^2, \quad (44)$$

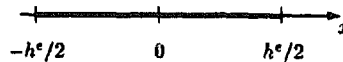


Fig. 1. The domain of a one-dimensional element.

$$\nabla w^h|_{\Omega^e} = a_1 + 2a_2x, \quad (45)$$

$$\Delta w^h|_{\Omega^e} = 2a_2, \quad (46)$$

and hence

$$\|\Delta w^h\|_{\Omega^e}^2 = \int_{-h^e/2}^{h^e/2} (\Delta w^h)^2 dx = 4a_2^2 h^e, \quad (47)$$

$$\|\nabla w^h\|_{\Omega^e}^2 = a_1^2 h^e + a_2^2 \frac{(h^e)^3}{3} \geq a_2^2 \frac{(h^e)^3}{3} = \frac{(h^e)^2}{12} \|\Delta w^h\|_{\Omega^e}^2, \quad (48)$$

so that $C_l = 12$.

For cubic elements ($l = 3$)

$$w^h|_{\Omega^e} = a_0 + a_1x + a_2x^2 + a_3x^3. \quad (49)$$

We find \bar{w}^h that satisfies (39) from

$$0 = \int_{-h^e/2}^{h^e/2} \nabla w^h dx = a_1 + a_3 \frac{(h^e)^2}{4}. \quad (50)$$

Substituting $a_1 = -a_3(h^e)^2/4$ into (49) yields

$$\bar{w}^h|_{\Omega^e} = a_0 - a_3 \frac{(h^e)^2}{4} x + a_2x^2 + a_3x^3, \quad (51)$$

and hence

$$\|\Delta w^h\|_{\Omega^e}^2 = h^e(4a_2^2 + 3a_3^2(h^e)^2), \quad (52)$$

$$\begin{aligned} \|\nabla w^h\|_{\Omega^e}^2 &= \|\nabla \bar{w}^h\|_{\Omega^e}^2 + \frac{h^e}{16} (4a_1 + a_3(h^e)^2)^2 \\ &\geq \|\nabla \bar{w}^h\|_{\Omega^e}^2 \\ &= \frac{(h^e)^3}{60} (20a_2^2 + 3a_3^2(h^e)^2) \\ &\geq \frac{(h^e)^2}{60} \|\Delta w^h\|_{\Omega^e}^2, \end{aligned} \quad (53)$$

so that $C_l = 60$.

For quartic elements ($l = 4$),

$$w^h|_{\Omega^e} = a_0 + a_1x + a_2x^2 + a_3x^3 + a_4x^4. \quad (54)$$

The function \bar{w}^h is obtained from w^h by the same procedure as in the case of cubic elements,

$$\bar{w}^h|_{\Omega^e} = a_0 - a_3 \frac{(h^e)^2}{4} x + a_2x^2 + a_3x^3 + a_4x^4, \quad (55)$$

and hence

$$\|\Delta w^h\|_{\Omega^e}^2 = \frac{h^e}{5} (20a_2^2 + 20a_2a_4(h^e)^2 + 15a_3^2(h^e)^2 + 9a_4^2(h^e)^4), \quad (56)$$

$$\begin{aligned} \|\nabla w^h\|_{\Omega^e}^2 &= \|\nabla \bar{w}^h\|_{\Omega^e}^2 + \frac{h^e}{16} (4a_1 + a_3(h^e)^2)^2 \\ &\geq \|\nabla \bar{w}^h\|_{\Omega^e}^2 \\ &= \frac{(h^e)^3}{420} (140a_2^2 + 84a_2a_4(h^e)^2 + 21a_3^2(h^e)^2 + 15a_4^2(h^e)^4). \end{aligned} \quad (57)$$

A bound may be obtained from the above equations, but deriving a sharp constant is quite difficult even in this one-dimensional case, requiring a considerable amount of ingenuity. Alternatively, and more simply, the sharpest bound is obtained from the eigenvalue problem

$$\left(\frac{h^e}{5} \begin{bmatrix} 20 & 0 & 10 \\ 0 & 15 & 0 \\ 10 & 0 & 9 \end{bmatrix} - \lambda^h \frac{(h^e)^3}{420} \begin{bmatrix} 140 & 0 & 42 \\ 0 & 21 & 0 \\ 42 & 0 & 15 \end{bmatrix} \right) \begin{Bmatrix} a_2 \\ a_3 h^e \\ a_4 (h^e)^2 \end{Bmatrix} = \mathbf{0}, \quad (58)$$

for which the maximum eigenvalue is

$$\lambda^h = \frac{2}{(h^e)^2} (45 + \sqrt{1605}). \quad (59)$$

The results in one dimension are summarized in Table 1.

Right isosceles triangles: Two-dimensional estimates are of practical importance. The interior of a right isosceles triangle of side h^e (Fig. 2) is the element domain, and again we examine the restriction of finite element functions and their derivatives to that domain. For linear elements ($l = 1$) the constant is again trivial since

$$w^h|_{\Omega^e} = a_0 + a_1x + a_2y, \quad (60)$$

which implies that $\Delta w^h|_{\Omega^e} = 0$ and hence $C_l = 0$.

For quadratic elements ($l = 2$)

$$w^h|_{\Omega^e} = a_0 + a_1x + a_2y + a_3x^2 + a_4xy + a_5y^2, \quad (61)$$

$$\nabla w^h|_{\Omega^e} = \begin{Bmatrix} a_1 + 2a_3x + a_4y \\ a_2 + a_4x + 2a_5y \end{Bmatrix}, \quad (62)$$

$$\Delta w^h|_{\Omega^e} = 2(a_3 + a_5). \quad (63)$$

Table 1

Values of the constant C_l in the inverse estimate of the advection-diffusion equation (36) in one dimension

l	C_l
1	0
2	12
3	60
4	$2(45 + \sqrt{1605})^a$

^a $C_4 \approx 170.1$.

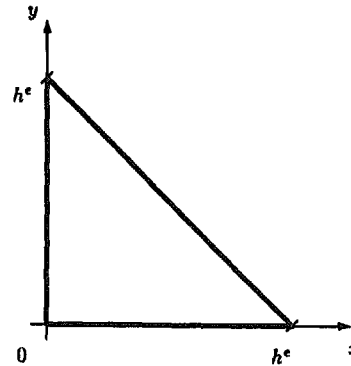


Fig. 2. The element domain of a right isosceles triangle.

We find \bar{w}^h that satisfies (39) from

$$\mathbf{0} = \int_{\Omega^e} \nabla w^h \, d\Omega = \frac{(h^e)^2}{6} \begin{Bmatrix} 3a_1 + 2a_3h^e + a_4h^e \\ 3a_2 + a_4h^e + 2a_5h^e \end{Bmatrix}. \quad (64)$$

Substituting for a_1 and a_2 into (61) yields

$$\bar{w}^h|_{\Omega^e} = a_0 + a_3 \left(x - \frac{2h^e}{3} \right) x + a_4 \left(xy - \frac{h^e}{3} x - \frac{h^e}{3} y \right) + a_5 \left(y - \frac{2h^e}{3} \right) y, \quad (65)$$

and hence

$$\|\Delta w^h\|_{\Omega^e}^2 = 2(h^e)^2(a_3 + a_5)^2, \quad (66)$$

$$\begin{aligned} \|\nabla w^h\|_{\Omega^e}^2 &= \|\nabla \bar{w}^h\|_{\Omega^e}^2 + \frac{(h^e)^2}{18} ((3a_1 + 2a_3h^e + a_4h^e)^2 + (3a_2 + a_4h^e + 2a_5h^e)^2) \\ &\geq \|\nabla \bar{w}^h\|_{\Omega^e}^2 \\ &= \frac{(h^e)^4}{18} (2a_3^2 - a_3a_4 + a_4^2 + a_4a_5 + 2a_5^2) \\ &= \frac{(h^e)^4}{72} ((a_3 - 2a_4 + a_5)^2 + 4(a_3 - a_5)^2 + 3(a_3 + a_5)^2) \\ &\geq \frac{(h^e)^4}{24} (a_3 + a_5)^2 \\ &= \frac{(h^e)^2}{48} \|\Delta w^h\|_{\Omega^e}^2. \end{aligned} \quad (67)$$

The fourth line of (67) demonstrates the degree of ingenuity in algebraic manipulation required to obtain sharp estimates. The maximum of the Rayleigh quotient is obtained at $a_4 = \frac{1}{2}(a_3 + a_5)$ and $a_3 = a_5$ (note correspondence to the first two terms in parentheses in the fourth line above), with the value $\lambda^h = 48/(h^e)^2$, verifying in a straightforward manner that the above result is indeed the lowest possible upper bound.

This case is already quite complicated, and evaluating the constant for cubic elements ($l = 3$) is significantly more difficult. The variational characterization, similar to (58), is virtually indispensable in this case. The details of this calculation are not presented, but the result is included in Table 2.

Straight-edged triangles: Consider the element domain to be a straight-edged triangle (with

Table 2
Values of the constant C_l in the inverse estimate of the advection-diffusion equation (36) for right isosceles triangles

l	C_l
1	0
2	48
3	$(435 + \sqrt{26025})/4^a$

^a $C_3 \approx 149.1$.

mid-nodes, if any, equally-spaced so that the Jacobian is constant), with vertex coordinates $\{x_a\}_{a=1}^3$, where $x_a = (x_a, y_a)$. The area of the element is

$$A = \frac{1}{2} \det \begin{bmatrix} 1 & x_1 & y_1 \\ 1 & x_2 & y_2 \\ 1 & x_3 & y_3 \end{bmatrix}. \quad (68)$$

For these elements exact integration of monomials in triangular coordinates (see [33, pp. 164–172]) may be employed. Alternatively, the following integration formulae are valid when the origin of the x - y coordinate system is located at the centroid of the triangle:

$$\int_{\Omega^e} d\Omega = A, \quad (69)$$

$$\int_{\Omega^e} x d\Omega = 0, \quad (70)$$

$$\int_{\Omega^e} y d\Omega = 0, \quad (71)$$

$$\int_{\Omega^e} x^2 d\Omega = \frac{A}{12} \sum_{a=1}^3 x_a^2, \quad (72)$$

$$\int_{\Omega^e} y^2 d\Omega = \frac{A}{12} \sum_{a=1}^3 y_a^2, \quad (73)$$

$$\int_{\Omega^e} xy d\Omega = \frac{A}{12} \sum_{a=1}^3 x_a y_a. \quad (74)$$

For linear elements ($l = 1$) the constant is trivial, as before. For quadratic elements ($l = 2$) the function, its gradient and Laplacian are given in (61), (62) and (63), respectively. We find \bar{w}^h that satisfies (39) from

$$0 = \int_{\Omega^e} \nabla w^h d\Omega = A \begin{Bmatrix} a_1 \\ a_2 \end{Bmatrix}. \quad (75)$$

Substituting for a_1 and a_2 into (61) yields

$$\bar{w}^h|_{\Omega^e} = a_0 + a_3 x^2 + a_4 xy + a_5 y^2, \quad (76)$$

and hence

$$\|\Delta w^h\|_{\Omega^e}^2 = 4A(a_3 + a_5)^2, \quad (77)$$

$$\begin{aligned} \|\nabla w^h\|_{\Omega^e}^2 &= \|\nabla \bar{w}^h\|_{\Omega^e}^2 + A(a_1^2 + a_2^2) \\ &\geq \|\nabla \bar{w}^h\|_{\Omega^e}^2 \\ &= \frac{A}{12} \left((4a_3^2 + a_4^2) \sum_{a=1}^3 x_a^2 + 4a_4(a_3 + a_5) \sum_{a=1}^3 x_a y_a + (a_4^2 + 4a_5^2) \sum_{a=1}^3 y_a^2 \right). \end{aligned} \quad (78)$$

The maximum of the Rayleigh quotient is obtained at

$$a_4 \left(\sum_{a=1}^3 x_a^2 + \sum_{a=1}^3 y_a^2 \right) = -2(a_3 + a_5) \sum_{a=1}^3 x_a y_a, \quad a_3 \sum_{a=1}^3 x_a^2 = a_5 \sum_{a=1}^3 y_a^2,$$

with the value

$$\lambda^h = 12 \frac{\sum_{a=1}^3 x_a^2 + \sum_{a=1}^3 y_a^2}{\sum_{a=1}^3 x_a^2 \sum_{a=1}^3 y_a^2 - \left(\sum_{a=1}^3 x_a y_a \right)^2} = \left(\frac{3}{A} \right)^2 \left(\sum_{a=1}^3 x_a^2 + \sum_{a=1}^3 y_a^2 \right), \quad (79)$$

where the coincidence of the origin with the centroid was employed to derive the second line above. Maintaining consistency with the value of the constant obtained for the quadratic right isosceles triangle (see Table 2) leads to a general definition of the element size (without restricting the location of the origin) in terms of the element area and the average vertex-to-centroid distance (all completely defined by the vertex coordinates), namely

$$h^e := \frac{4A}{\sqrt{3 \sum_{a=1}^3 |x_a - x_c|^2}}, \quad (80)$$

where x_c are the centroid coordinates. This definition takes into account certain aspects of element distortion (for example, in the limit of an ‘arbitrarily thin’ right triangle, i.e., when one of the interior angles tends to zero, the element size h^e tends to the *smaller* side multiplied by $\sqrt{2}$, see Fig. 3), is not costly to compute and may be incorporated in finite element methods that employ parameters that depend on the mesh size.

Squares: The element domain is a square of side h^e with its center at the origin (Fig. 4), i.e., $\Omega^e =]-h^e/2, h^e/2[\times]-h^e/2, h^e/2[$. For bilinear elements ($l = 1$) the constant is again trivial since

$$w^h|_{\Omega^e} = a_0 + a_1 x + a_2 y + a_3 xy, \quad (81)$$

implying that $\Delta w^h|_{\Omega^e} = 0$ and hence $C_l = 0$.

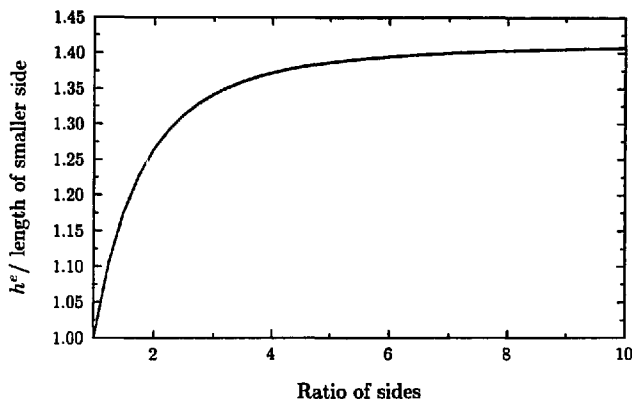


Fig. 3. Element size of a quadratic right triangle in advection-diffusion, derived from (80). (This figure also holds for quadratic rectangles, see discussion of (94).)

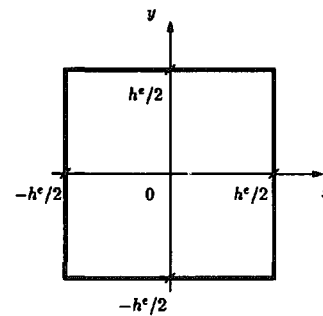


Fig. 4. The domain of a square element.

For biquadratic squares ($l = 2$),

$$w^h|_{\Omega^e} = a_0 + a_1x + a_2y + a_3x^2 + a_4xy + a_5y^2 + a_6x^2y + a_7xy^2 + a_8x^2y^2, \quad (82)$$

$$\nabla w^h|_{\Omega^e} = \begin{Bmatrix} a_1 + 2a_3x + a_4y + 2a_6xy + a_7y^2 + 2a_8xy^2 \\ a_2 + a_4x + 2a_5y + a_6x^2 + 2a_7xy + 2a_8x^2y \end{Bmatrix}, \quad (83)$$

$$\Delta w^h|_{\Omega^e} = 2(a_3 + a_5 + a_6y + a_7x + a_8(x^2 + y^2)). \quad (84)$$

We find \bar{w}^h that satisfies (39) from

$$\mathbf{0} = \int_{\Omega^e} \nabla w^h \, d\Omega = \frac{(h^e)^2}{12} \begin{Bmatrix} 12a_1 + a_7(h^e)^2 \\ 12a_2 + a_6(h^e)^2 \end{Bmatrix}. \quad (85)$$

Substituting for a_1 and a_2 into (82) yields

$$\bar{w}^h|_{\Omega^e} = a_0 + a_3x^2 + a_4xy + a_5y^2 + a_6\left(x^2 - \frac{(h^e)^2}{12}\right)y + a_7\left(y^2 - \frac{(h^e)^2}{12}\right)x + a_8x^2y^2, \quad (86)$$

and hence

$$\begin{aligned} \|\Delta w^h\|_{\Omega^e}^2 &= \frac{(h^e)^2}{45} (180a_3^2 + 180a_5^2 + 360a_3a_5 + 15a_6^2(h^e)^2 + 15a_7^2(h^e)^2 \\ &\quad + 7a_8^2(h^e)^4 + 60a_3a_8(h^e)^2 + 60a_5a_8(h^e)^2), \\ \|\nabla w^h\|_{\Omega^e}^2 &= \|\nabla \bar{w}^h\|_{\Omega^e}^2 + \frac{(h^e)^2}{144} ((12a_1 + a_7(h^e)^2)^2 + (12a_2 + a_6(h^e)^2)^2) \\ &\geq \|\nabla \bar{w}^h\|_{\Omega^e}^2 \\ &= \frac{(h^e)^4}{360} (120a_3^2 + 60a_4^2 + 120a_5^2 + 12a_6^2(h^e)^2 + 12a_7^2(h^e)^2 \\ &\quad + 3a_8^2(h^e)^4 + 20a_3a_8(h^e)^2 + 20a_5a_8(h^e)^2) \\ &= \frac{(h^e)^4}{1080} (5(6a_3 + 6a_5 + a_8(h^e)^2)^2 + 180(a_3 - a_5)^2 + 180a_4^2 \\ &\quad + 36a_6^2(h^e)^2 + 36a_7^2(h^e)^2 + 4a_8^2(h^e)^4) \\ &\geq \frac{(h^e)^4}{1080} (5(6a_3 + 6a_5 + a_8(h^e)^2)^2 + 15a_6^2(h^e)^2 + 15a_7^2(h^e)^2 + 2a_8^2(h^e)^4) \\ &= \frac{(h^e)^2}{24} \|\Delta w^h\|_{\Omega^e}^2. \end{aligned} \quad (88)$$

This result is corroborated (circumventing the complexity of algebraic manipulation above) by estimating the constant variationally, yielding $\lambda^h = 24/(h^e)^2$.

The constant for the bicubic square ($l = 3$) was characterized variationally yielding the result presented in Table 3.

Rectangles: In this case, the element domain is a rectangle of sides h_x and h_y , with its

Table 3

Values of the constant C_l in the inverse estimate of the advection-diffusion equation (36) for square elements

l	C_l
1	0
2	24
3	$(244 + \sqrt{9136})/3^a$

^a $C_3 \approx 113.2$.

center at the origin, i.e., $\Omega^e =]-h_x/2, h_x/2[\times]-h_y/2, h_y/2[$. For bilinear rectangles ($l = 1$) the constant is trivial, as before.

For biquadratic rectangles ($l = 2$) the function, its gradient and Laplacian are given in (82), (83) and (84), respectively. We find \bar{w}^h that satisfies (39) from

$$\mathbf{0} = \int_{\Omega^e} \nabla w^h \, d\Omega = \frac{h_x h_y}{12} \begin{Bmatrix} 12a_1 + a_7 h_y^2 \\ 12a_2 + a_6 h_x^2 \end{Bmatrix}. \quad (89)$$

Substituting for a_1 and a_2 into (82) yields

$$\bar{w}^h|_{\Omega^e} = a_0 + a_3 x^2 + a_4 xy + a_5 y^2 + a_6 \left(x^2 - \frac{h_x^2}{12} \right) y + a_7 \left(y^2 - \frac{h_y^2}{12} \right) x + a_8 x^2 y^2, \quad (90)$$

and hence

$$\begin{aligned} \|\Delta w^h\|_{\Omega^e}^2 &= \frac{h_x h_y}{180} (720a_3^2 + 720a_5^2 + 1440a_3a_5 + 60a_6^2 h_y^2 + 60a_7^2 h_x^2 \\ &\quad + a_8^2(9h_x^4 + 10h_x^2 h_y^2 + 9h_y^4) + 120a_3a_8(h_x^2 + h_y^2) + 120a_5a_8(h_x^2 + h_y^2)), \\ \|\nabla w^h\|_{\Omega^e}^2 &= \|\nabla \bar{w}^h\|_{\Omega^e}^2 + \frac{h_x h_y}{144} ((12a_1 + a_7 h_y^2)^2 + (12a_2 + a_6 h_x^2)^2) \\ &\geq \|\nabla \bar{w}^h\|_{\Omega^e}^2 \\ &= \frac{h_x h_y}{720} (240a_3^2 h_x^2 + 60a_4^2 (h_x^2 + h_y^2) + 240a_5^2 h_y^2 + 4a_6^2 h_x^2 (h_x^2 + 5h_y^2) \\ &\quad + 4a_7^2 h_y^2 (5h_x^2 + h_y^2) + 3a_8^2 h_x^2 h_y^2 (h_x^2 + h_y^2 + 40a_3a_8 h_x^2 h_y^2 + 40a_5a_8 h_x^2 h_y^2)). \end{aligned} \quad (91)$$

Characterizing the constant variationally yields a maximum value of the Rayleigh quotient of

$$\lambda^h = 12 \frac{h_x^2 + h_y^2}{h_x^2 h_y^2}. \quad (93)$$

Maintaining consistency with the value of the constant obtained for biquadratic squares (see Table 3) leads to a more general definition of the element size in terms of the element area and the radius of the circumscribing circle, namely

$$h^e := h_x h_y \sqrt{\frac{2}{h_x^2 + h_y^2}}. \quad (94)$$

This simple definition accounts for the element aspect ratio in precisely the same manner that (80) accounted for distortion of right triangles (in the limit of an 'infinitely stretched' rectangle the element size h^e also tends to the smaller side multiplied by $\sqrt{2}$, see Fig. 3) and may be incorporated in finite element methods that employ parameters that depend on the mesh size.

3.2. Elasticity

The equations of isotropic incompressible elasticity are identical to the equations of Stokes flow. Examples of the application of inverse estimates to these problems are found in [3, 4, 12, 18, 19, 22]. In the elasticity problem, $w: \bar{\Omega} \rightarrow \mathbb{R}^d$ are the displacements, and the strains are

$$\epsilon(w) := \frac{1}{2} (\nabla w + \nabla w^t). \quad (95)$$

The strains bound their divergence in this version of the inequality

$$(h^e)^2 \|\operatorname{div} \epsilon(w^h)\|_{\Omega^e}^2 \leq C_l \|\epsilon(w^h)\|_{\Omega^e}^2 \quad \forall w^h \in \mathcal{V}^h. \quad (96)$$

As in the case of the advection-diffusion problem, global statements of this inequality are possible. The one-dimensional case for this problem is identical to the one-dimensional case of the advective-diffusive inequality (36).

Right isosceles triangles: The element domain is again a right triangle of side h^e (Fig. 2). For linear elements ($l = 1$) the constant is again trivial since

$$w^h|_{\Omega^e} = \begin{Bmatrix} a_0 + a_1 x + a_2 y \\ b_0 + b_1 x + b_2 y \end{Bmatrix}, \quad (97)$$

$$\epsilon(w^h)|_{\Omega^e} = \begin{bmatrix} a_1 & \frac{1}{2}(a_2 + b_1) \\ \text{symm.} & b_2 \end{bmatrix}. \quad (98)$$

In this case $\operatorname{div} \epsilon(w^h)|_{\Omega^e} = 0$ and hence $C_l = 0$.

For quadratic elements ($l = 2$)

$$w^h|_{\Omega^e} = \begin{Bmatrix} a_0 + a_1 x + a_2 y + a_3 x^2 + a_4 xy + a_5 y^2 \\ b_0 + b_1 x + b_2 y + b_3 x^2 + b_4 xy + b_5 y^2 \end{Bmatrix}, \quad (99)$$

$$\epsilon(w^h)|_{\Omega^e} = \begin{bmatrix} a_1 + 2a_3 x + a_4 y & \frac{1}{2}(a_2 + a_4 x + 2a_5 y + b_1 + 2b_3 + b_4 y) \\ \text{symm.} & b_2 + b_4 x + 2b_5 y \end{bmatrix}, \quad (100)$$

$$\operatorname{div} \epsilon(w^h)|_{\Omega^e} = \begin{Bmatrix} 2a_3 + a_5 + \frac{1}{2}b_4 \\ \frac{1}{2}a_4 + b_3 + 2b_5 \end{Bmatrix}. \quad (101)$$

We reduce the number of independent coefficients in the functions, cf. (39), by considering

$$\begin{aligned} 0 &= \int_{\Omega^e} \epsilon(w^h) d\Omega \\ &= \frac{(h^e)^2}{6} \begin{bmatrix} 3a_1 + 2a_3 h^e + a_4 h^e & \frac{1}{2}(3a_2 + a_4 h^e + 2a_5 h^e + 3b_1 + 2b_3 h^e + b_4 h^e) \\ \text{symm.} & 3b_2 + b_4 h^e + 2b_5 h^e \end{bmatrix}. \end{aligned} \quad (102)$$

Substituting for a_1 , a_2 , b_1 and b_2 in (99) yields

$$\bar{w}^h|_{\Omega^e} = \begin{Bmatrix} a_0 + a_3(x - 2h^e/3)x + a_4(xy - xh^e/3 - yh^e/3) + a_5(y - 2h^e/3)y \\ b_0 + b_3(x - 2h^e/3)x + b_4(xy - xh^e/3 - yh^e/3) + b_5(y - 2h^e/3)y \end{Bmatrix}, \quad (103)$$

and hence

$$\|\operatorname{div} \epsilon(w^h)\|_{\Omega^e}^2 = \frac{(h^e)^2}{2} ((2a_3 + a_5 + \frac{1}{2}b_4)^2 + (\frac{1}{2}a_4 + b_3 + 2b_5)^2), \quad (104)$$

$$\begin{aligned} \|\epsilon(w^h)\|_{\Omega^e}^2 &= \|\epsilon(\bar{w}^h)\|_{\Omega^e}^2 + \frac{(h^e)^2}{36} (2(3a_1 + 2a_3h^e + a_4h^e)^2 + 2(3b_2 + b_4h^e + 2b_5h^e)^2 \\ &\quad + (3a_2 + a_4h^e + 2a_5h^e + 3b_1 + 2b_3h^e + b_4h^e)^2) \\ &\geq \|\epsilon(\bar{w}^h)\|_{\Omega^e}^2 \\ &= \frac{(h^e)^4}{72} (8a_3^2 + 3a_4^2 + 4a_5^2 + 4b_3^2 + 3b_4^2 + 8b_5^2 - 4a_3a_4 - 2a_4a_5 \\ &\quad + 4a_4b_3 - a_4b_4 - 4a_5b_3 + 4a_5b_4 - 2b_3b_4 - 4b_4b_5). \end{aligned} \quad (105)$$

Characterizing the constant variationally yields a maximum value of the Rayleigh quotient of $\lambda^h = 42/(h^e)^2$. The constant $C_l = 42$ is lower than the corresponding value for the advection-diffusion inequality (cf. Table 2) for $l = 2$.

The constant for the cubic triangle ($l = 3$) was characterized variationally and evaluated numerically, yielding the result presented in Table 4 (which, again, is lower than the corresponding value obtained for the inverse inequality of advection-diffusion).

Straight-edged triangles: As before we consider the element domain to be a straight-edge triangle (with mid-nodes, if any, equally-spaced so that the Jacobian is constant), with vertex coordinates $\{x_a\}_{a=1}^3$, where $x_a = (x_a, y_a)$. The element area is given in (68), and integration formulae (69)–(74) apply when the origin coincides with the centroid of the triangle.

For linear elements ($l = 1$) the constant is trivial, as before. For quadratic elements ($l = 2$) the function, the strain and its divergence are given in (99), (100) and (101), respectively. Again we consider

$$0 = \int_{\Omega^e} \epsilon(w^h) d\Omega = \begin{bmatrix} a_1 & \frac{1}{2}(a_2 + b_1) \\ \text{symm.} & a_2 \end{bmatrix}. \quad (106)$$

Substituting for a_1 , a_2 , b_1 and b_2 into (99) yields

$$\bar{w}^h|_{\Omega^e} = \begin{Bmatrix} a_0 + a_3x^2 + a_4xy + a_5y^2 \\ b_0 + b_3x^2 + b_4xy + b_5y^2 \end{Bmatrix}, \quad (107)$$

Table 4

Values of the constant C_l in the elasticity inverse estimate (96) for right isosceles triangles

l	C_l
1	0
2	42
3	103.7 ^a

^a C_3 was evaluated numerically.

and hence

$$\|\operatorname{div} \epsilon(w^h)\|_{\Omega^e}^2 = A((2a_3 + a_5 + \frac{1}{2}b_4)^2 + (\frac{1}{2}a_4 + b_3 + 2b_5)^2) \quad (108)$$

$$\begin{aligned} \|\epsilon(w^h)\|_{\Omega^e}^2 &= \|\epsilon(\bar{w}^h)\|_{\Omega^e}^2 + \frac{A}{2} (2a_1^2 + 2b_2^2 + (a_2 + b_1)^2) \\ &\geq \|\epsilon(\bar{w}^h)\|_{\Omega^e}^2 \\ &= \frac{A}{24} \left((8a_3^2 + 2b_4^2 + (a_4 + 2b_3)^2) \sum_{a=1}^3 x_a^2 + (2a_4^2 + 8b_5^2 + (2a_5 + b_4)^2) \sum_{a=1}^3 y_a^2 \right. \\ &\quad \left. + 2(4(a_3a_4 + b_4b_5) + (a_4 + 2b_3)(2a_5 + b_4)) \sum_{a=1}^3 x_a y_a \right). \end{aligned} \quad (109)$$

The maximum value of the Rayleigh quotient is

$$\begin{aligned} \lambda^h &= 3 \frac{3 \left(\sum_{a=1}^3 x_a^2 + \sum_{a=1}^3 y_a^2 \right) + \sqrt{4 \left(\sum_{a=1}^3 x_a y_a \right)^2 + \left(\sum_{a=1}^3 x_a^2 - \sum_{a=1}^3 y_a^2 \right)^2}}{\sum_{a=1}^3 x_a^2 \sum_{a=1}^3 y_a^2 - \left(\sum_{a=1}^3 x_a y_a \right)^2} \\ &= \left(\frac{3}{2A} \right)^2 \left(3 \left(\sum_{a=1}^3 x_a^2 + \sum_{a=1}^3 y_a^2 \right) + \sqrt{\left(\sum_{a=1}^3 x_a^2 + \sum_{a=1}^3 y_a^2 \right)^2 - \frac{16A^2}{3}} \right), \end{aligned} \quad (110)$$

where the coincidence of the origin with the centroid was employed to derive the second line above. As for the right isosceles triangle, this value is lower than the corresponding one for the advection-diffusion inequality, cf. (79). Again, a more general definition of the element size that accounts for distortion in terms of the element area and the average vertex-to-centroid distance

$$h^e := \sqrt{\frac{56A^2/3}{3 \sum_{a=1}^3 |x_a - x_c|^2 + \sqrt{\left(\sum_{a=1}^3 |x_a - x_c|^2 \right)^2 - 16A^2/3}}} \quad (111)$$

(completely determined by the vertex coordinates, with no restriction on the location of the element origin) is obtained by maintaining consistency with the value $C_l = 42$ obtained for the quadratic right isosceles triangle. (In this case the limit of an ‘arbitrarily thin’ right triangle leads to an element size that tends to the smaller side multiplied by $\sqrt{7}/4$. See comparison to the case of advection-diffusion in Fig. 5.) This definition is still inexpensive to compute and may be incorporated in finite element methods that require mesh-dependent parameters. Alternatively, the values obtained for the advection-diffusion case (see Table B.1 in Appendix B) may be employed as conservative estimates for these expressions.

Squares: Again the element domain is a square of side h^e with its center at the origin (Fig. 4), i.e., $\Omega^e =]-h^e/2, h^e/2[\times]-h^e/2, h^e/2[$, and finite element functions and their derivatives are restricted to that domain. For the first time the constant for bilinear squares ($l = 1$) is non-trivial since the contribution of the bilinear term is not eliminated from the divergence of strain,

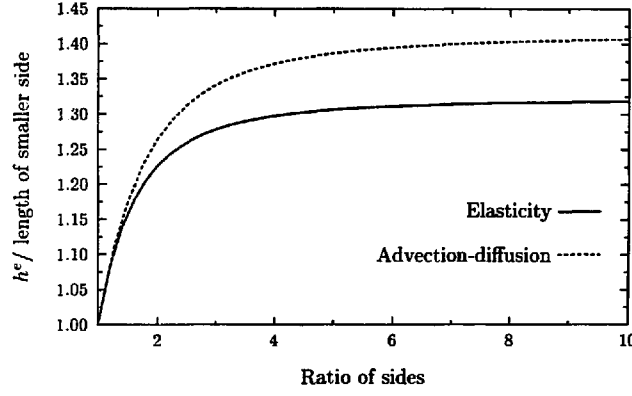


Fig. 5. Element size of a quadratic right triangle in elasticity, derived from (111), in comparison to advection-diffusion, derived from (80).

$$\mathbf{w}^h|_{\Omega^e} = \begin{Bmatrix} a_0 + a_1x + a_2y + a_3xy \\ b_0 + b_1x + b_2y + b_3xy \end{Bmatrix}, \quad (112)$$

$$\boldsymbol{\epsilon}(\mathbf{w}^h)|_{\Omega^e} = \begin{bmatrix} a_1 + a_3y & \frac{1}{2}(a_2 + a_3x + b_1 + b_3y) \\ \text{symm.} & b_2 + b_3x \end{bmatrix}, \quad (113)$$

$$\text{div } \boldsymbol{\epsilon}(\mathbf{w}^h)|_{\Omega^e} = \frac{1}{2} \begin{Bmatrix} b_3 \\ a_3 \end{Bmatrix}. \quad (114)$$

We reduce the number of independent coefficients in the functions, cf. (39), by considering

$$\mathbf{0} = \int_{\Omega^e} \boldsymbol{\epsilon}(\mathbf{w}^h) d\Omega = (h^e)^2 \begin{bmatrix} a_1 & \frac{1}{2}(a_2 + b_1) \\ \text{symm.} & b_2 \end{bmatrix}. \quad (115)$$

Substituting for a_1 , a_2 , b_1 and b_2 in (112) yields

$$\bar{\mathbf{w}}^h|_{\Omega^e} = \begin{Bmatrix} a_0 + a_3xy \\ b_0 + b_3xy \end{Bmatrix}, \quad (116)$$

and hence

$$\|\text{div } \boldsymbol{\epsilon}(\mathbf{w}^h)\|_{\Omega^e}^2 = \frac{(h^e)^2}{4} (a_3^2 + b_3^2), \quad (117)$$

$$\begin{aligned} \|\boldsymbol{\epsilon}(\mathbf{w}^h)\|_{\Omega^e}^2 &= \|\boldsymbol{\epsilon}(\bar{\mathbf{w}}^h)\|_{\Omega^e}^2 + \frac{(h^e)^2}{2} (2a_1^2 + (a_2 + b_1)^2 + 2b_2^2) \\ &\geq \|\boldsymbol{\epsilon}(\bar{\mathbf{w}}^h)\|_{\Omega^e}^2 \\ &= \frac{(h^e)^4}{8} (a_3^2 + b_3^2) \\ &= \frac{(h^e)^2}{2} \|\text{div } \boldsymbol{\epsilon}(\mathbf{w}^h)\|_{\Omega^e}^2, \end{aligned} \quad (118)$$

so that $C_l = 2$. This leads to the expectation that, contrary to the behavior observed in triangular elements, here the values of the constant will be higher than the corresponding ones for the advection-diffusion equation.

For biquadratic squares ($l = 2$)

$$\mathbf{w}^h|_{\Omega^e} = \begin{Bmatrix} a_0 + a_1x + a_2y + a_3x^2 + a_4xy + a_5y^2 + a_6x^2y + a_7xy^2 + a_8x^2y^2 \\ b_0 + b_1x + b_2y + b_3x^2 + b_4xy + b_5y^2 + b_6x^2y + b_7xy^2 + b_8x^2y^2 \end{Bmatrix}. \quad (119)$$

We reduce the number of independent coefficients in the functions, cf. (39), by considering

$$\begin{aligned} \mathbf{0} &= \int_{\Omega^e} \boldsymbol{\epsilon}(\mathbf{w}^h) d\Omega \\ &= \frac{(h^e)^2}{12} \begin{bmatrix} 12a_1 + a_7(h^e)^2 & \frac{1}{2}(12a_2 + a_6(h^e)^2 + 12b_1 + b_7(h^e)^2) \\ \text{symm.} & 12b_2 + b_6(h^e)^2 \end{bmatrix}. \end{aligned} \quad (120)$$

Substituting for a_1 , a_2 , b_1 and b_2 in (119) yields

$$\bar{\mathbf{w}}^h|_{\Omega^e} = \begin{Bmatrix} a_0 + a_3x^2 + a_4xy + a_5y^2 + a_6\left(x^2 - \frac{(h^e)^2}{12}\right)y + a_7\left(y^2 - \frac{(h^e)^2}{12}\right)x + a_8x^2y^2 \\ b_0 + b_3x^2 + b_4xy + b_5y^2 + b_6\left(x^2 - \frac{(h^e)^2}{12}\right)y + b_7\left(y^2 - \frac{(h^e)^2}{12}\right)x + b_8x^2y^2 \end{Bmatrix}, \quad (121)$$

and hence

$$\begin{aligned} \|\operatorname{div} \boldsymbol{\epsilon}(\mathbf{w}^h)\|_{\Omega^e}^2 &= \frac{(h^e)^2}{144} (576a_3^2 + 36a_4^2 + 144a_5^2 + 60a_6^2(h^e)^2 + 24a_7^2(h^e)^2 + 17a_8^2(h^e)^4 \\ &\quad + 144b_3^2 + 36b_4^2 + 576b_5^2 + 24b_6^2(h^e)^2 + 60b_7^2(h^e)^2 \\ &\quad + 17b_8^2(h^e)^4 + 576a_3a_5 + 288a_3b_4 + 144a_4b_3 + 288a_4b_5 \\ &\quad + 144a_5b_4 + 576b_3b_5 + 144a_3a_8(h^e)^2 + 36a_4b_8(h^e)^2 \\ &\quad + 72a_5a_8(h^e)^2 + 96a_6b_7(h^e)^2 + 48a_7b_6(h^e)^2 + 36a_8b_4(h^e)^2 \\ &\quad + 72b_3b_8(h^e)^2 + 144b_5b_8(h^e)^2), \end{aligned} \quad (122)$$

$$\begin{aligned} \|\boldsymbol{\epsilon}(\mathbf{w}^h)\|_{\Omega^e}^2 &= \|\boldsymbol{\epsilon}(\bar{\mathbf{w}}^h)\|_{\Omega^e}^2 + \frac{(h^e)^2}{288} (2(12a_1 + a_7(h^e)^2)^2 + 2(12b_2 + b_6(h^e)^2)^2 \\ &\quad + (12a_2 + a_6(h^e)^2 + 12b_1 + b_7(h^e)^2)^2) \\ &\geq \|\boldsymbol{\epsilon}(\bar{\mathbf{w}}^h)\|_{\Omega^e}^2 \\ &= \frac{(h^e)^4}{1440} (480a_3^2 + 180a_4^2 + 240a_5^2 + 44a_6^2(h^e)^2 + 28a_7^2(h^e)^2 + 9a_8^2(h^e)^4 \\ &\quad + 240b_3^2 + 180b_4^2 + 480b_5^2 + 28b_6^2(h^e)^2 + 44b_7^2(h^e)^2 + 9b_8^2(h^e)^4 \\ &\quad + 240a_4b_3 + 240a_5b_4 + 40a_5a_8(h^e)^2 + 40a_7b_6(h^e)^2 \\ &\quad + 20a_8b_4(h^e)^2 + 40b_3b_8(h^e)^2). \end{aligned} \quad (123)$$

Evaluating the constant is rather complex. The details of the calculation are not presented, but the result, obtained by the variational characterization, is $C_l = 270/11$ (≈ 24.5). This value is

again larger than the corresponding constant for the advection-diffusion equation (cf. Table 3).

Rectangles: Again, consider the element domain to be a rectangle of sides h_x and h_y , with its center at the origin, i.e., $\Omega^e =]-h_x/2, h_x/2[\times]-h_y/2, h_y/2[$. For bilinear elements ($l = 1$) the function, the strain and its divergence are given in (112), (113) and (114), respectively. Again we consider

$$\mathbf{0} = \int_{\Omega^e} \boldsymbol{\epsilon}(\mathbf{w}^h) d\Omega = h_x h_y \begin{bmatrix} a_1 & \frac{1}{2}(a_2 + b_1) \\ \text{symm.} & b_2 \end{bmatrix}, \quad (124)$$

so that $\bar{\mathbf{w}}^h$ is given in (116).

$$\|\text{div } \boldsymbol{\epsilon}(\mathbf{w}^h)\|_{\Omega^e}^2 = \frac{h_x h_y}{4} (a_3^2 + b_3^2), \quad (125)$$

$$\begin{aligned} \|\boldsymbol{\epsilon}(\mathbf{w}^h)\|_{\Omega^e}^2 &= \|\boldsymbol{\epsilon}(\bar{\mathbf{w}}^h)\|_{\Omega^e}^2 + \frac{h_x h_y}{2} (2a_1^2 + (a_1 + b_1)^2 + 2b_2^2) \\ &\geq \|\boldsymbol{\epsilon}(\bar{\mathbf{w}}^h)\|_{\Omega^e}^2 \\ &= \frac{h_x h_y}{24} (a_3^2(h_x^2 + 2h_y^2) + b_3^2(2h_x^2 + h_y^2)) \\ &\geq \min\{h_x^2 + 2h_y^2, 2h_x^2 + h_y^2\} \frac{h_x h_y}{24} (a_3^2 + b_3^2) \\ &= \frac{\min\{h_x^2 + 2h_y^2, 2h_x^2 + h_y^2\}}{6} \|\text{div } \boldsymbol{\epsilon}(\mathbf{w}^h)\|_{\Omega^e}^2, \end{aligned} \quad (126)$$

maintaining $C_l = 2$ with

$$h^e = \sqrt{\frac{h_x^2 + h_y^2 + \min\{h_x^2, h_y^2\}}{3}}, \quad (127)$$

which takes into account the element aspect ratio. (See Fig. 6. In contrast to previous cases, the limit of an “infinitely stretched” rectangle leads to an element size that tends to the *larger* side divided by $\sqrt{3}$, probably due to the influence of the bilinear term evident in this inverse estimate.)

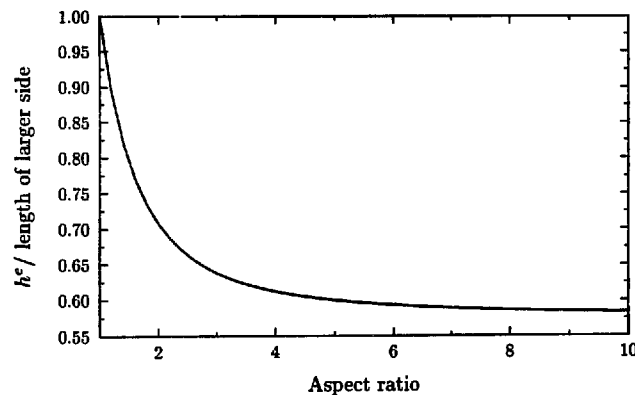


Fig. 6. Element size of a linear rectangle in elasticity, see (127).

Evaluation of the constant for biquadratic rectangles ($l=2$) requires quite elaborate calculations, which are not presented. The largest value of the Rayleigh quotient is

$$\lambda^h = 15 \left(\frac{(h_x^2 + h_y^2)(4h_x^4 + 47h_x^2h_y^2 + 4h_y^4)}{h_x^2h_y^2(h_x^2 + 10h_y^2)(10h_x^2 + h_y^2)} + \frac{\sqrt{(h_x^2 + h_y^2)^2(4h_x^4 + 47h_x^2h_y^2 + 4h_y^4)^2 - 36h_x^4h_y^4(h_x^2 + 10h_y^2)(10h_x^2 + h_y^2)}}{h_x^2h_y^2(h_x^2 + 10h_y^2)(10h_x^2 + h_y^2)} \right), \quad (128)$$

and a generalization of the definition of element size may be derived.

3.3. Reissner–Mindlin plate theory

Problems of shear-deformable plate bending are described by Reissner–Mindlin theory, where $\theta : \bar{\Omega} \rightarrow \mathbb{R}^2$ are the transverse rotations and the curvature tensor is

$$\kappa(\theta) := \frac{1}{2} (\nabla \theta + \nabla \theta^t). \quad (129)$$

The moments are

$$m(\theta) = -c^b \kappa(\theta), \quad (130)$$

where $c^b = [c_{\alpha\beta\gamma\delta}^b]$ is the tensor of bending moduli ($1 \leq \alpha, \beta, \gamma, \delta \leq 2$). In the nondimensional isotropic case this tensor takes on the explicit form

$$c_{\alpha\beta\gamma\delta}^b = \frac{1}{2} (\delta_{\alpha\gamma}\delta_{\beta\delta} + \delta_{\alpha\delta}\delta_{\beta\gamma}) + \frac{\nu}{1-\nu} \delta_{\alpha\beta}\delta_{\gamma\delta}, \quad (131)$$

where $\delta_{\alpha\beta}$ is the Kronecker delta and ν is Poisson's ratio ($-1 < \nu < 1/2$, so that the elasticity tensor is positive definite). The inverse estimate for Reissner–Mindlin plate theory states that curvatures bound the divergence of moments,

$$(h^e)^2 \|\operatorname{div} m(\theta^h)\|_{\Omega^e}^2 \leq C_l \|\kappa(\theta^h)\|_{\Omega^e}^2 \quad \forall \theta^h \in \mathcal{V}^h. \quad (132)$$

This version of the inverse estimate is employed in [20].

Right isosceles triangles: The element domain is again a right isosceles triangle of side h^e (Fig. 2). For linear elements ($l=1$) the constant is again trivial, see (98).

For quadratic elements ($l=2$)

$$\theta^h|_{\Omega^e} = \begin{Bmatrix} a_0 + a_1x + a_2y + a_3x^2 + a_4xy + a_5y^2 \\ b_0 + b_1x + b_2y + b_3x^2 + b_4xy + b_5y^2 \end{Bmatrix}, \quad (133)$$

$$\kappa(\theta^h)|_{\Omega^e} = \begin{bmatrix} a_1 + 2a_3x + a_4y & \frac{1}{2}(a_2 + a_4x + 2a_5y + b_1 + 2b_3 + b_4y) \\ \text{symm.} & b_2 + b_4x + 2b_5y \end{bmatrix}, \quad (134)$$

$$\operatorname{div} m(\theta^h)|_{\Omega^e} = \frac{1}{1-\nu} \begin{Bmatrix} 2a_3 + (1-\nu)a_5 + \frac{1}{2}(1+\nu)b_4 \\ \frac{1}{2}(1+\nu)a_4 + (1-\nu)b_3 + 2b_5 \end{Bmatrix}. \quad (135)$$

We reduce the number of independent coefficients in the functions, cf. (39), by considering

$$\begin{aligned}
\mathbf{0} &= \int_{\Omega^e} \boldsymbol{\kappa}(\boldsymbol{\theta}^h) d\Omega \\
&= \frac{(h^e)^2}{6} \left[\begin{array}{c} 3a_1 + 2a_3h^e + a_4h^e \\ \text{symm.} \end{array} \quad \begin{array}{c} \frac{1}{2}(3a_2 + a_4h^e + 2a_5h^e + 3b_1 + 2b_3h^e + b_4h^e) \\ 3b_2 + b_4h^e + 2b_5h^e \end{array} \right]. \quad (136)
\end{aligned}$$

Substituting for a_1 , a_2 , b_1 and b_2 in (133) yields

$$\bar{\boldsymbol{\theta}}^h|_{\Omega^e} = \left\{ \begin{array}{l} a_0 + a_3(x - 2h^e/3)x + a_4(xy - xh^e/3 - yh^e/3) + a_5(y - 2h^e/3)y \\ b_0 + b_3(x - 2h^e/3)x + b_4(xy - xh^e/3 - yh^e/3) + b_5(y - 2h^e/3)y \end{array} \right\}, \quad (137)$$

and hence

$$\begin{aligned}
\|\operatorname{div} \mathbf{m}(\boldsymbol{\theta}^h)\|_{\Omega^e}^2 &= \frac{(h^e)^2}{2(1-\nu)^2} ((2a_3 + (1-\nu)a_5 + \frac{1}{2}(1+\nu)b_4)^2 \\
&\quad + \frac{1}{2}((1+\nu)a_4 + (1-\nu)b_3 + 2b_5)^2), \quad (138)
\end{aligned}$$

$$\begin{aligned}
\|\boldsymbol{\kappa}(\boldsymbol{\theta}^h)\|_{\Omega^e}^2 &= \|\boldsymbol{\kappa}(\bar{\boldsymbol{\theta}}^h)\|_{\Omega^e}^2 + \frac{(h^e)^2}{36} (2(3a_1 + 2a_3h^e + a_4h^e)^2 + 2(3b_2 + b_4h^e + 2b_5h^e)^2 \\
&\quad + (3a_2 + a_4h^e + 2a_5h^e + 3b_1 + 2b_3h^e + b_4h^e)^2) \\
&\geq \|\boldsymbol{\kappa}(\bar{\boldsymbol{\theta}}^h)\|_{\Omega^e}^2 \\
&= \frac{(h^e)^4}{72} (8a_3^2 + 3a_4^2 + 4a_5^2 + 4b_3^2 + 3b_4^2 + 8b_5^2 - 4a_3a_4 - 2a_4a_5 \\
&\quad + 4a_4b_3 - a_4b_4 - 4a_5b_3 + 4a_5b_4 - 2b_3b_4 - 4b_4b_5). \quad (139)
\end{aligned}$$

Characterizing the constant variationally yields a maximum value of the Rayleigh quotient of

$$\lambda^h = \frac{6(7 - 2\nu + 7\nu^2)}{(1-\nu)^2(h^e)^2}. \quad (140)$$

The constant $C_l = 42 + 72\nu/(1-\nu)^2$ is equal to the corresponding value for the elasticity inequality at $\nu = 0$, cf. Table 4, for $l=2$. Larger values of Poisson's ratio have a significant affect on the constant (Fig. 7). For example, $\nu = 0.3$ (typical of engineering materials) increases the constant by over 100% and in the incompressible limit ($\nu \rightarrow 0.5$) $C_l = 186$.

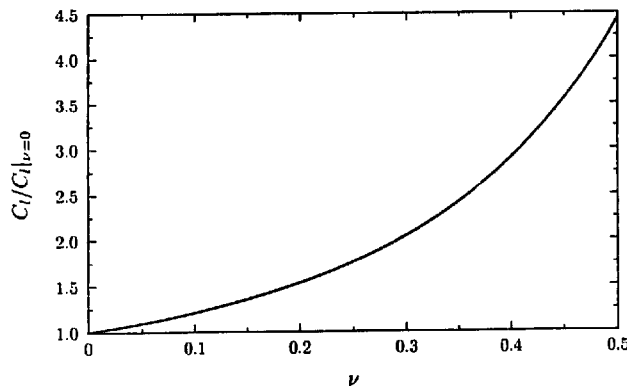


Fig. 7. Coefficient of the inverse estimate for a quadratic isosceles triangle ($l=2$) in Reissner–Mindlin plate theory.

Straight-edged triangles: We again consider the element domain to be the straight-edged triangle described previously. The element area is given in (68), and integration formulae (69)–(74) apply when the origin coincides with the centroid of the triangle.

For linear elements ($l = 1$) the constant is trivial, as before. For quadratic elements ($l = 2$) the function, the curvature and the moment divergence are given in (133), (134) and (135), respectively. Again we consider

$$\mathbf{0} = \int_{\Omega^e} \boldsymbol{\kappa}(\boldsymbol{\theta}^h) d\Omega = A \begin{bmatrix} a_1 & \frac{1}{2}(a_2 + b_1) \\ \text{symm.} & a_2 \end{bmatrix}. \quad (141)$$

Substituting for a_1 , a_2 , b_1 and b_2 into (99) yields

$$\bar{\boldsymbol{\theta}}^h|_{\Omega^e} = \begin{Bmatrix} a_0 + a_3x^2 + a_4xy + a_5y^2 \\ b_0 + b_3x^2 + b_4xy + b_5y^2 \end{Bmatrix}, \quad (142)$$

and hence

$$\|\text{div } \mathbf{m}(\boldsymbol{\theta}^h)\|_{\Omega^e}^2 = \frac{A}{(1-\nu)^2} ((2a_3 + (1-\nu)a_5 + (1+\nu)b_4/2)^2 + ((1+\nu)a_4/2 + (1-\nu)b_3 + 2b_5)^2), \quad (143)$$

$$\begin{aligned} \|\boldsymbol{\kappa}(\boldsymbol{\theta}^h)\|_{\Omega^e}^2 &= \|\boldsymbol{\kappa}(\bar{\boldsymbol{\theta}}^h)\|_{\Omega^e}^2 + \frac{A}{2} (2a_1^2 + 2b_2^2 + (a_2 + b_1)^2) \\ &\geq \|\boldsymbol{\kappa}(\bar{\boldsymbol{\theta}}^h)\|_{\Omega^e}^2 \\ &= \frac{A}{24} \left((8a_3^2 + 2b_4^2 + (a_4 + 2b_3)^2) \sum_{a=1}^3 x_a^2 + (2a_4^2 + 8b_5^2 + (2a_5 + b_4)^2) \sum_{a=1}^3 y_a^2 \right. \\ &\quad \left. + 2(4(a_3a_4 + b_4b_5) + (a_4 + 2b_3)(2a_5 + b_4)) \sum_{a=1}^3 x_a y_a \right). \end{aligned} \quad (144)$$

The maximum value of the Rayleigh quotient is

$$\begin{aligned} \lambda^h &= \left(\frac{3}{2(1-\nu)A} \right)^2 \left((3-2\nu+3\nu^2) \left(\sum_{a=1}^3 x_a^2 + \sum_{a=1}^3 y_a^2 \right) \right. \\ &\quad \left. + (1+\nu)^2 \sqrt{\left(\sum_{a=1}^3 x_a^2 + \sum_{a=1}^3 y_a^2 \right)^2 - \frac{16A^2}{3}} \right), \end{aligned} \quad (145)$$

leading to a generalization of the definition of the quadratic element size (111) which accounts for the effect of Poisson's ratio in the inverse estimate

$$h^e := \sqrt{\frac{8(7-2\nu+7\nu^2)A^2/3}{(3-2\nu+3\nu^2) \sum_{a=1}^3 |x_a - x_c|^2 + (1+\nu)^2 \sqrt{\left(\sum_{a=1}^3 |x_a - x_c|^2 \right)^2 - 16A^2/3}}}. \quad (146)$$

The element size of a right isosceles triangle is unaffected by the value of Poisson's ratio. Recall that for an 'arbitrarily thin' right triangle the element size tends to the smaller side multiplied by $\sqrt{7/4}$ when $\nu = 0$. A value of $\nu = 0.3$ reduces this by only 8%, and in the incompressible limit it is reduced by 11%.

Squares: Again the element domain is a square of side h^e with its center at the origin (Fig. 4). The constant for bilinear squares ($l = 1$) is nontrivial as before since

$$\theta^h|_{\Omega^e} = \begin{Bmatrix} a_0 + a_1x + a_2y + a_3xy \\ b_0 + b_1x + b_2y + b_3xy \end{Bmatrix}, \quad (147)$$

$$\kappa(\theta^h)|_{\Omega^e} = \begin{bmatrix} a_1 + a_3y & \frac{1}{2}(a_2 + a_3x + b_1 + b_3y) \\ \text{symm.} & b_2 + b_3x \end{bmatrix}, \quad (148)$$

$$\text{div } m(\theta^h)|_{\Omega^e} = \frac{1+\nu}{2(1-\nu)} \begin{Bmatrix} b_3 \\ a_3 \end{Bmatrix}. \quad (149)$$

We reduce the number of independent coefficients in the functions, cf. (39), by considering

$$\mathbf{0} = \int_{\Omega^e} \kappa(\theta^h) d\Omega = (h^e)^2 \begin{bmatrix} a_1 & \frac{1}{2}(a_2 + b_1) \\ \text{symm.} & b_2 \end{bmatrix}. \quad (150)$$

Substituting for a_1 , a_2 , b_1 and b_2 in (147) yields

$$\bar{\theta}^h|_{\Omega^e} = \begin{Bmatrix} a_0 + a_3xy \\ b_0 + b_3xy \end{Bmatrix}, \quad (151)$$

and hence

$$\|\text{div } m(\theta^h)\|_{\Omega^e}^2 = \frac{(1+\nu)^2(h^e)^2}{4(1-\nu)^2} (a_3^2 + b_3^2), \quad (152)$$

$$\begin{aligned} \|\kappa(\theta^h)\|_{\Omega^e}^2 &= \|\kappa(\bar{\theta}^h)\|_{\Omega^e}^2 + \frac{(h^e)^2}{2} (2a_1^2 + (a_2 + b_1)^2 + 2b_2^2) \\ &\geq \|\kappa(\bar{\theta}^h)\|_{\Omega^e}^2 \\ &= \frac{(h^e)^4}{8} (a_3^2 + b_3^2) \\ &= \frac{(1-\nu)^2(h^e)^2}{2(1+\nu)^2} \|\text{div } m(\theta^h)\|_{\Omega^e}^2, \end{aligned} \quad (153)$$

so that $C_l = 2 + 8\nu/(1-\nu)^2$ is again equal to the corresponding value for the elasticity inequality at $\nu = 0$. Increasing Poisson's ratio leads to a dramatic increase in the value of the coefficient.

The coefficient for the biquadratic square ($l = 2$) was characterized variationally, yielding

$$C_l = \frac{30(3+\nu)^2}{11(1-\nu)^2}, \quad \nu > 0. \quad (154)$$

(Other eigenvalues dominate in part of the range $-1 < \nu < 0$.) Again, the value of the coefficient is sensitive to Poisson's ratio. Figure 8 shows the dependence of the coefficients for bilinear and biquadratic squares on Poisson's ratio.

Rectangles: Consider the element domain to be a rectangle of sides h_x and h_y , with its center at the origin, i.e., $\Omega^e =]-h_x/2, h_x/2[\times]-h_y/2, h_y/2[$, and restriction of finite element functions and their derivatives to that domain. For bilinear elements ($l = 1$) the function, the

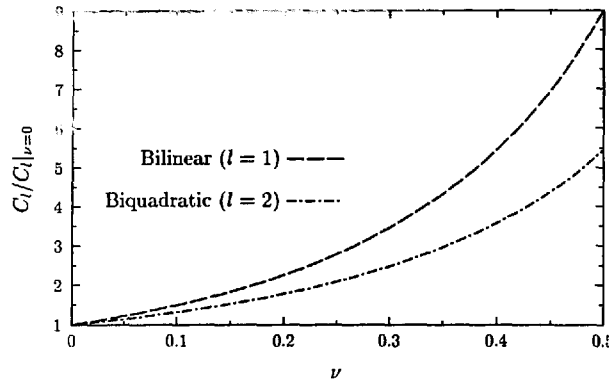


Fig. 8. Coefficient of the inverse estimate for squares in Reissner–Mindlin plate theory.

curvature and the moment divergence are given in (147), (148) and (149), respectively. Again we consider

$$\mathbf{0} = \int_{\Omega^e} \boldsymbol{\kappa}(\boldsymbol{\theta}^h) \, d\Omega = h_x h_y \begin{bmatrix} a_1 & \frac{1}{2}(a_2 + b_1) \\ \text{symm.} & b_2 \end{bmatrix}, \quad (155)$$

so that $\bar{\boldsymbol{\theta}}^h$ is given in (151).

$$\|\text{div } \mathbf{m}(\boldsymbol{\theta}^h)\|_{\Omega^e}^2 = \frac{(1+\nu)^2 h_x h_y}{4(1-\nu)^2} (a_3^2 + b_3^2), \quad (156)$$

$$\begin{aligned} \|\boldsymbol{\kappa}(\boldsymbol{\theta}^h)\|_{\Omega^e}^2 &= \|\boldsymbol{\kappa}(\bar{\boldsymbol{\theta}}^h)\|_{\Omega^e}^2 + \frac{h_x h_y}{2} (2a_1^2 + (a_2 + b_1)^2 + 2b_2^2) \\ &\geq \|\boldsymbol{\kappa}(\bar{\boldsymbol{\theta}}^h)\|_{\Omega^e}^2 \\ &= \frac{h_x h_y}{24} (a_3^2 (h_x^2 + 2h_y^2) + b_3^2 (2h_x^2 + h_y^2)) \\ &\geq \min\{h_x^2 + 2h_y^2, 2h_x^2 + h_y^2\} \frac{h_x h_y}{24} (a_3^2 + b_3^2) \\ &= \min\{h_x^2 + 2h_y^2, 2h_x^2 + h_y^2\} \frac{(1-\nu)^2 (h^e)^2}{6(1+\nu)^2} \|\text{div } \mathbf{m}(\boldsymbol{\theta}^h)\|_{\Omega^e}^2, \end{aligned} \quad (157)$$

maintaining $C_l = 2 + 8\nu/(1-\nu)^2$ with h^e defined in (127) (see Fig. 6).

4. Least-squares bounds

An extension of inverse estimates was recently derived in [25] for the analysis of Galerkin/least-squares methods for problems of time-harmonic acoustics. These inequalities, called least-squares bounds (in the original work the name ‘norm equivalence of the Helmholtz operator’ was used), explicate the advantageous effect of Galerkin/least-squares terms in enhancing stability of various formulations. As in the case of inverse estimates, least-squares bounds hold for finite-dimensional function spaces and emanate from element-level inequalities. Prior to [25], error analysis of Galerkin/least-squares methods relied on inverse estimates such as (36). In such analyses, the Galerkin/least-squares term was

decomposed via the left-hand inequality of (A.4) in Appendix A, and then the inverse estimate was employed to demonstrate control over destabilizing terms. The least-squares bounds achieve this result more directly, and, in general, provide a sharper estimate. Indeed, the inverse estimate may not suffice to prove stability for the Helmholtz operator in the entire range of propagating phenomena, whereas the least-squares bounds were successfully employed in this end in [25]. Least-squares bounds might be used in the mathematical analysis of other applications in which Galerkin/least-squares methods have proved successful, such as advective-diffusive equations (see Section 4.2) and mixed problems.

4.1. Time-harmonic acoustics

The Helmholtz operator is

$$\mathcal{L}w := \Delta w + k^2 w, \quad (158)$$

where $w : \bar{\Omega} \rightarrow \mathbb{C}$ is the Fourier coefficient of the acoustic pressure or velocity potential and k is the wave number. We assume the following least-squares bounds of the Helmholtz operator hold $\forall k^2 \in \mathbb{R}$:

$$L_{kh} \|\mathcal{L}w^h\|_{\Omega^e}^2 \leq k^4 \|w^h\|_{\Omega^e}^2 \leq U_{kh} \|\mathcal{L}w^h\|_{\Omega^e}^2 \quad \forall w^h \in \mathcal{V}^h. \quad (159)$$

In support of the plausibility of (159) we note that $\|\mathcal{L}w^h\|_{\Omega^e}$ is indeed a norm since no piecewise polynomial satisfies the Helmholtz equation. Furthermore, we have calculated the coefficients for several elements. In general, the coefficients $L_{kh} \leq 1 \leq U_{kh}$ depend on the numerically nondimensionalized wave number kh and the degree of interpolation. For notational simplicity we suppress the dependence on the individual element e , but as (159) indicates we still emphasize the local nature of this inequality. All the cases that were evaluated were actually found to depend on $(kh)^4$, i.e., to be symmetric with respect to $(kh)^2$ and behave identically in propagation and decay (which correspond to positive and negative k^2 , respectively). The coefficients may be characterized by their asymptotic behavior

$$\left. \begin{array}{l} L_{kh} \rightarrow 1 \\ U_{kh} \rightarrow 1 \end{array} \right\} \quad \text{as } (kh)^2 \rightarrow \pm\infty, \quad (160)$$

$$\left. \begin{array}{l} L_{kh} \rightarrow 0 \\ U_{kh} \rightarrow \infty \end{array} \right\} \quad \text{as } (kh)^2 \rightarrow 0. \quad (161)$$

For all linear elements $\Delta w^h|_{\Omega^e} = 0$ and hence $L_{kh} \equiv U_{kh} \equiv 1$.

One dimension: As before, consider the element domain to be an open interval (Fig. 1), and consider finite element functions and their derivatives restricted to that domain. In this case explicit expressions for the coefficients are easily obtained. The upper bound is

$$U_{kh} = 1 + \frac{C_l}{2(kh)^4} + \sqrt{\frac{C_l}{2(kh)^4} \left(2 + \frac{C_l}{2(kh)^4}\right)}, \quad (162)$$

where $C_l \geq 0$ is a nondimensional constant that depends only on the degree of interpolation l (and is independent of h , increases monotonically with l for any family of elements, and in general $C_l \rightarrow \infty$ as $l \rightarrow \infty$, as in the case of the inverse estimate). The coefficient is estimated by

$$1 + \frac{C_l}{(kh)^4} \leq U_{kh} \leq 2 + \frac{C_l}{(kh)^4} \quad \forall k^2 \in \mathbb{R}. \quad (163)$$

The lower bound is

$$L_{kh} = \frac{1}{U_{kh}}. \quad (164)$$

We have calculated values of the constant C_l for elements with $l \leq 4$ (see Table 5). An example of U_{kh} is depicted in Fig. 9, with its inverse L_{kh} and its bounds. Since (162) and (163) depend on $(kh)^4$, the results are symmetric with respect to $(kh)^2$, as shown in the figure.

Right isosceles triangles: The element domain is the interior of a right isosceles triangle (Fig. 2). For linear elements the coefficients both equal identity, as previously noted. For the quadratic triangle $L_{kh} = 1/U_{kh}$ as in the one-dimensional case, and (162) and its estimate (163) hold with $C_l = 5040$.

Squares: Again the element domain is a square with its center at the origin (Fig. 4). For bilinear squares the coefficients both equal identity, as previously noted. The coefficients of the biquadratic square are the extremal solutions of a cubic equation. Explicit expressions for these coefficients are not presented, but the coefficients are estimated as follows:

$$1 + \frac{C_l}{(kh)^4} \leq L_{kh}^{-1} \leq 2 + \frac{2C_l}{(kh)^4}, \quad (165)$$

$$1 + \frac{2C_l}{(kh)^4} + \frac{C_l^2}{(kh)^8} \leq U_{kh} \leq 2 + \frac{3C_l}{(kh)^4} + \frac{C_l^2}{(kh)^8}, \quad (166)$$

where $C_l = 1440$. The coefficients and these estimates are shown in Fig. 10.

Rectangles: The element domain is a rectangle of sides h_x and h_y with its center at the origin. The coefficients for rectangles of various aspect ratios are presented in Fig. 11.

4.2. Other applications

The steady advection-diffusion operator reduces in one dimension to

$$\mathcal{L}w := aw_{,x} - \kappa w_{,xx}, \quad (167)$$

where $w : \bar{\Omega} \rightarrow \mathbb{R}$, a is the given flow velocity and $\kappa > 0$ is the diffusivity, assumed constant. The statement of the least-squares bounds for the one-dimensional advection-diffusion operator is

Table 5

Values of the constant C_l in the definition (162) of the coefficient U_{kh} in the least-squares bounds of the Helmholtz equation (159) in one dimension

l	C_l
1	0 ^a
2	720
3	9120
4	58800

^a $U_{kh} \equiv 1$ for linear elements.

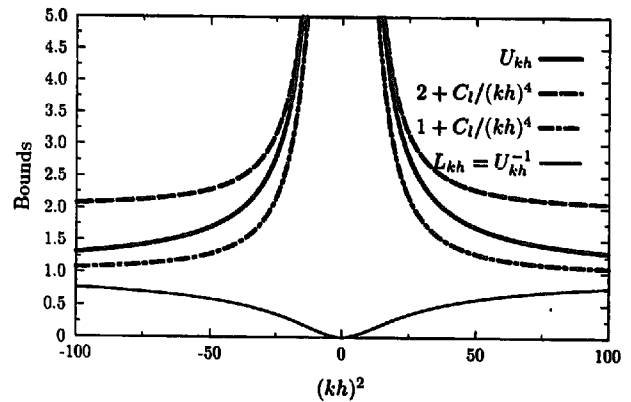


Fig. 9. Least-squares bounds in one dimension: quadratic elements ($C_l = 720$).

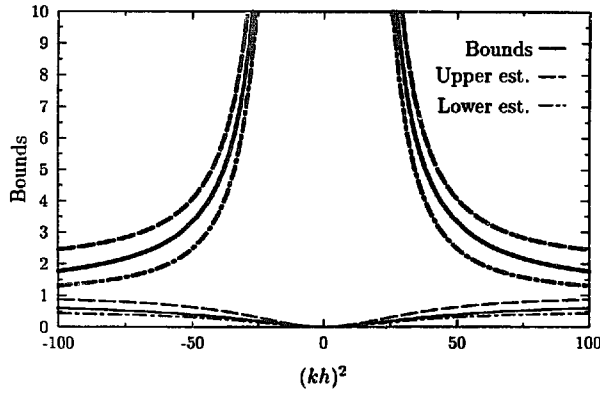


Fig. 10. Least-squares bounds for biquadratic squares (the bold lines correspond to the upper bound U_{kh}).

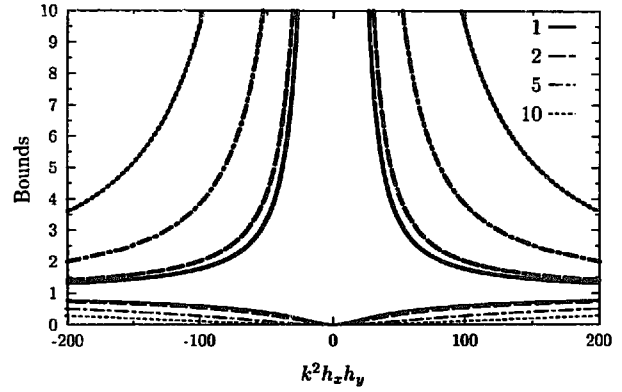


Fig. 11. Least-squares bounds for biquadratic rectangles of varying aspect ratios (the bold lines correspond to the upper bound U_{kh}).

$$\frac{1}{B_\alpha} \|\mathcal{L}w^h\|_{\Omega^e}^2 \leq \alpha^2 \|w^h\|_{\Omega^e}^2 \leq B_\alpha \|\mathcal{L}w^h\|_{\Omega^e}^2 \quad \forall w^h \in \mathcal{V}^h. \quad (168)$$

In general, the coefficient $B_\alpha \geq 1$ depends on the element Peclet number $\alpha = ah^e/(2\kappa)$ and the degree of interpolation. All the cases that were evaluated were found to depend on α^2 , i.e., to be insensitive to the direction of the given flow. The asymptotic behavior in the advective limit is

$$B_\alpha \rightarrow 1 \quad \text{as } \alpha \rightarrow \infty. \quad (169)$$

For linear elements $w^h_{,xx}|_{\Omega^e} = 0$ and hence $B_\alpha \equiv 1$. For quadratic elements

$$B_\alpha = 1 + \frac{3}{2\alpha^2} + \sqrt{\frac{3}{2\alpha^2} \left(2 + \frac{3}{2\alpha^2}\right)}. \quad (170)$$

The striking similarity to the coefficient in the inequality for the one-dimensional Helmholtz operator (162) does not continue for higher-order elements.

The generalization of this inequality to the multi-dimensional advection-diffusion operator is not as straightforward as was the case for the time-harmonic acoustic problem due to the directionality inherent in the operator. Since there are piecewise polynomials that satisfy the multi-dimensional advection-diffusion equation, $\|\mathcal{L}w^h\|_{\Omega^e}$ violates the definiteness requirement of a norm. The inequality in this case must therefore be stated with care.

5. Conclusions

In this work we have investigated inequalities that are employed in the analysis of finite element methods. Poincaré–Friedrichs inequalities, inverse estimates and least-square bounds were examined. A detailed characterization of these inequalities is particularly pertinent to the construction of new classes of finite element formulations that are designed on the basis of error analysis.

We have improved known results for Poincaré–Friedrichs inequalities for arbitrary multi-dimensional domains. These results were then specialized to annular regions leading to sharper estimates of the constant. Precise characterization of the boundary terms yielded a

generalization to Neumann problems. Overall we are not aware of earlier derivations of estimates as sharp as the ones presented herein.

Inverse estimates are frequently employed in the analysis of finite element methods. We have examined such inequalities for problems of advection-diffusion, incompressible elasticity (and Stokes flow) and shear-deformable plates. The mesh-dependent terms in formulations that contain such quantities often depend on the parameters of the inverse estimate. Since inverse estimates emanate from element-level inequalities their applicability is not restricted to quasi-uniform meshes. The sharpest possible values of the constant in the inequality were determined for several families of Lagrange elements over a range of degrees of interpolation for all of the applications mentioned above. Precise definitions of the element size were derived for several triangles and rectangles. These definitions take into account element aspect ratios and distortion and hence are not limited to regular elements. All of these results may be employed in methods that incorporate mesh-dependent parameters.

In a relatively recent development, least-squares bounds were employed in the analysis of finite element methods for problems of time-harmonic acoustics. These inequalities are similar in nature to inverse estimates. The characterization of least-squares bounds can also lead to improved definition of mesh-dependent terms. As in inverse estimates, these results are not limited to regular elements on quasi-uniform meshes. Multi-dimensional least-squares bounds are presented herein for the first time, accounting for aspect-ratio affects of rectangles. The range of applications in which these inequalities are used may be broadened in the future.

Appendix A. Basic inequalities

For reference purposes, several well-known inequalities are listed in the following. The notation (\cdot, \cdot) represents *any* mapping on a vector space into a scalar field that satisfies the properties of an inner product, and $\|\cdot\|$ is understood as the corresponding norm.

The Schwarz inequality states

$$|(x, y)| \leq \|x\| \|y\|. \quad (\text{A.1})$$

The triangle inequality follows from (A.1),

$$|\|x\| - \|y\|| \leq \|x + y\| \leq \|x\| + \|y\|. \quad (\text{A.2})$$

Since $\|x + y\|^2 \geq 0$,

$$-\epsilon \|x\|^2 - \frac{1}{\epsilon} \|y\|^2 \leq \pm 2 \operatorname{Re}(x, y) \leq \epsilon \|x\|^2 + \frac{1}{\epsilon} \|y\|^2 \quad \forall \epsilon > 0, \quad (\text{A.3})$$

and by (A.3),

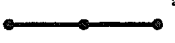
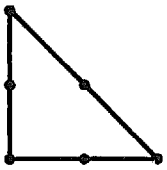
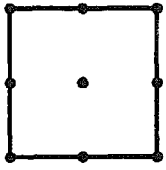
$$\frac{1}{1 + \epsilon} \|x\|^2 - \frac{1}{\epsilon} \|y\|^2 \leq \|x + y\|^2 \leq (1 + \epsilon) \|x\|^2 + \left(1 + \frac{1}{\epsilon}\right) \|y\|^2 \quad \forall \epsilon > 0. \quad (\text{A.4})$$

Appendix B. Summary of inverse estimates

The parameters obtained for inverse estimates for advection-diffusion (36), elasticity (96) and Reissner–Mindlin plates (132) are summarized in Tables B.1, B.2 and B.3, respectively. The case of one-dimensional elasticity is covered in Table B.1, since it is identical to

Table B.1

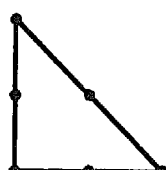
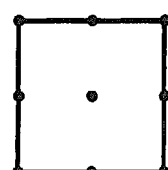
Summary of results for inverse estimates of the advection-diffusion equation (36)

  					
l	C_l	C_l	h^e	C_l	h^e
1	0	0	—	0	—
2	12	48	$\frac{4A}{\sqrt{3}s}$ ^b	24	$\frac{\sqrt{2}h_x h_y}{\sqrt{h_x^2 + h_y^2}}$ ^c
3	60	$\frac{435 + \sqrt{26025}}{4}$	—	$\frac{244 + \sqrt{9136}}{3}$	—
4	$2(45 + \sqrt{1605})$	—	—	—	—

^a For one-dimensional elements h^e is the element length.^b For straight-angled triangles, $s^2 = \sum_{a=1}^3 |\mathbf{x}_a - \mathbf{x}_c|^2$, where \mathbf{x}_a and \mathbf{x}_c are the coordinates of the vertices and the centroid, respectively; see discussion of eq. (80).^c For rectangles, see discussion of eq. (94).

Table B.2

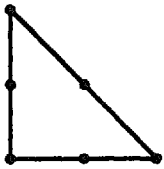
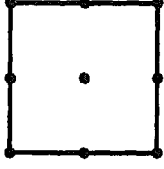
Summary of results for inverse estimates of elasticity (96) (the one-dimensional case is identical to advection-diffusion, see Table B.1)

				
l	C_l	h^e	C_l	h^e
1	0	—	2	$\sqrt{\frac{h_x^2 + h_y^2 + \min\{h_x^2, h_y^2\}}{3}}^a$
2	42	$\sqrt{\frac{56A^2/3}{3s^2 + \sqrt{s^4 - \frac{16A^2}{3}}}}^b$	$\frac{270}{11}$	— ^c
3	103.7	—	—	—

^a For rectangles, see discussion of eq. (127).^b For straight-angled triangles, $s^2 = \sum_{a=1}^3 |\mathbf{x}_a - \mathbf{x}_c|^2$, where \mathbf{x}_a and \mathbf{x}_c are the coordinates of the vertices and the centroid, respectively; see discussion of eq. (111).^c The largest eigenvalue of the quadratic rectangle is presented in (128). The element size may be derived from $(h^e)^2 = C_l/\lambda^h$.

Table B.3

Summary of results for inverse estimates of Reissner–Mindlin plate theory (132)

			
l	C_l	h^c	C_l h^c
1	0	–	$2 \frac{(1+\nu)^2}{(1-\nu)^2}$ ^a
2	$\frac{6(7-2\nu+7\nu^2)}{(1-\nu)^2}$	$\sqrt{\frac{8(7-2\nu+7\nu^2)A^2/3}{(3-2\nu+3\nu^2)s^2 + (1+\nu)^2\sqrt{s^4 - \frac{16A^2}{3}}}}$ ^b	$\frac{30(3+\nu)^2}{11(1-\nu)^2}$ –

^a Same as in Table B.2 for bilinear ($l=1$) rectangles.

^b For straight-edged triangles, $s^2 = \sum_{a=1}^3 |\mathbf{x}_a - \mathbf{x}_c|^2$, where \mathbf{x}_a and \mathbf{x}_c are the coordinates of the vertices and the centroid, respectively, see discussion of eq. (146).

advection-diffusion in one dimension. The element size of the bilinear rectangle for Reissner–Mindlin plates is identical to that of elasticity and is presented in Table B.2.

For any family of elements the constants of the inverse estimates for a given application increase monotonically in magnitude with increasing order of interpolation. The constants of the inverse estimates for triangles are higher than those for quadrilateral elements, and the one-dimensional inequalities have the lowest constants of all. In one dimension, advection-diffusion and elasticity inequalities are identical. In two dimensions, the advection-diffusion constants for triangles are higher than the corresponding constants for elasticity, whereas the advection-diffusion constants for quadrilateral elements are lower than the corresponding ones for elasticity, probably due to the nonvanishing contribution of the bilinear terms in elasticity. The coefficients for plates all reduce to the two-dimensional elasticity ones for $\nu = 0$. These coefficients are highly dependent on Poisson's ratio, as shown in Figs. 7 and 8.

Several definitions of element size that arise naturally in the context of the various applications were derived. In particular, definitions that account for distortion of straight-edged triangles and for aspect ratios of rectangular elements are presented and characterized graphically in Figs. 3, 5 and 6. For distorted triangles the element size according to these definitions tends to the smaller side (scaled by a constant of order one), and for stretched rectangles in advection-diffusion as well. But for rectangles in elasticity and plates the element size tends to the larger side (scaled by a constant of order one), probably due the contribution of the bilinear term.

These precise estimates of the coefficients and definitions of the element size in inverse estimates may be employed in the design of methods that contain mesh-dependent quantities.

Acknowledgment

This research was supported in part by the U.S. Office of Naval Research under Contracts N00014-89-K-0027 and N00014-88-K-0446. The authors are grateful to Leo Franca, whose ongoing interest in this work provided an impetus for its publication.

References

- [1] J. Douglas, Jr. and J. Wang, An absolutely stabilized finite element method for the Stokes flow, *Math. Comput.* 52 (1989) 495–508.
- [2] L.P. Franca and E.G. Dutra do Carmo, The Galerkin gradient least-squares method, *Comput. Methods Appl. Mech. Engrg.* 74 (1989) 41–54.
- [3] L.P. Franca, S.L. Frey and T.J.R. Hughes, Stabilized finite element methods: I. Application to the advective-diffusive model, *Comput. Methods Appl. Mech. Engrg.* 95 (1992) 253–276.
- [4] L.P. Franca and T.J.R. Hughes, Two classes of mixed finite element methods, *Comput. Methods Appl. Engrg.* 69 (1988) 89–129.
- [5] T.J.R. Hughes and F. Brezzi, On drilling degrees of freedom, *Comput. Methods Appl. Mech. Engrg.* 72 (1989) 105–121.
- [6] T.J.R. Hughes and A.N. Brooks, A multi-dimensional upwind scheme with no crosswind diffusion, in: T.J.R. Hughes, ed., *Finite Element Methods for Convection Dominated Flows*, AMD Vol. 34 (ASME, New York, 1979) 19–35.
- [7] T.J.R. Hughes, L.P. Franca and G.M. Hulbert, A new finite element formulation for computational fluid dynamics: VIII. The Galerkin/least-squares method for advective–diffusive equations, *Comput. Methods Appl. Mech. Engrg.* 73 (1989) 173–189.
- [8] T.J.R. Hughes and G.M. Hulbert, Space-time finite element methods for elastodynamics: Formulations and error estimates, *Comput. Methods Appl. Mech. Engrg.* 66 (1988) 339–363.
- [9] C. Johnson, Streamline diffusion methods for problems in fluid mechanics, in: R.H. Gallagher, G.F. Carey, J.T. Oden and O.C. Zienkiewicz, eds., *Finite Elements in Fluids—Vol. 6* (Wiley, Chichester, 1986) 251–261.
- [10] T.J.R. Hughes and M. Mallet, A new finite element formulation for computational fluid dynamics: III. The generalized streamline operator multidimensional advective–diffusive systems, *Comput. Methods Appl. Mech. Engrg.* 58 (1986) 305–328.
- [11] C. Johnson, U. Nävert and J. Pitkäranta, Finite element methods for linear hyperbolic problems, *Comput. Methods Appl. Mech. Engrg.* 45 (1984) 285–312.
- [12] T.J.R. Hughes, L.P. Franca and M. Balestra, A new finite element formulation for computational fluid dynamics: V. Circumventing the Babuška–Bezzi condition: A stable Petrov–Galerkin formulation of the Stokes problem accommodating equal-order interpolations, *Comput. Methods Appl. Mech. Engrg.* 59 (1986) 85–99.
- [13] T.J.R. Hughes, L.P. Franca, I. Harari, M. Mallet, F. Shakib and T.E. Spelce, Finite element methods for high-speed flows: Consistent calculation of boundary flux, *AIAA 25th Aerospace Sciences Meeting*, Paper no. 87-0556, Reno, Nevada, 1987.
- [14] T.J.R. Hughes and F. Shakib, Computational aerodynamics and the finite element method, *AIAA 26th Aerospace Sciences Meeting*, Paper no. 88-0031, Reno, Nevada, 1988.
- [15] C. Johnson and J. Saranen, Streamline diffusion methods for the incompressible Euler and Navier–Stokes equations, *Math. Comput.* 47 (1986) 1–18.
- [16] T.J.R. Hughes, Recent progress in the development and understanding of SUPG methods with special reference to the compressible Euler and Navier–Stokes equations, *Internat. J. Numer. Methods Engrg.* 7 (1987) 1261–1275.
- [17] C. Johnson, *Numerical Solutions of Partial Differential Equations by the Finite Element Method* (Cambridge Univ. Press, Cambridge, 1987).
- [18] T.J.R. Hughes and L.P. Franca, A new finite element formulation for computational fluid dynamics: VII. The Stokes problem with various well-posed boundary conditions: Symmetric formulations that converge for all velocity/pressure spaces, *Comput. Methods Appl. Mech. Engrg.* 65 (1987) 85–96.
- [19] L.P. Franca and R. Stenberg, Error analysis of some Galerkin/least-squares methods for the elasticity equations, *SIAM J. Numer. Anal.*, in press.
- [20] T.J.R. Hughes and L.P. Franca, A mixed finite element formulation for Reissner–Mindlin plate theory: Uniform convergence of all higher-order spaces, *Comput. Methods Appl. Mech. Engrg.* 67 (1988) 223–240.
- [21] H.J.C. Barbosa and T.J.R. Hughes, The finite element method with Lagrange multipliers on the boundary: Circumventing the Babuška–Brezzi condition, *Comput. Methods Appl. Mech. Engrg.* 85 (1991) 109–128.
- [22] L.P. Franca, Analysis and finite element approximation of compressible and incompressible linear isotropic elasticity based upon a variational principle, *Comput. Methods Appl. Mech. Engrg.* 76 (1989) 259–273.
- [23] T.J.R. Hughes, F. Frezzi, A. Masud and I. Harari, Finite elements with drilling degrees of freedom: Theory and numerical evaluations, in: R. Gruber, J. Periaux and R.P. Shaw, eds., *Proceedings of the fifth International Symposium on Numerical Methods in Engineering*, Vol. 1 (Springer, Berlin, 1989) 3–17.

- [24] I. Harari and T.J.R. Hughes, Design and analysis of finite element methods for the Helmholtz equation in exterior domains, *Appl. Mech. Rev.* 43 (1990) 366–373.
- [25] I. Harari and T.J.R. Hughes, A cost comparison of boundary element and finite element methods for problems of time harmonic acoustics, *Comput. Methods Appl. Mech. Engrg.* 97 (1992) 77–102.
- [26] D.J. Silvester and N. Kechkar, Stabilised bilinear–constant velocity–pressure finite elements for the conjugate gradient solution of the Stokes problem, *Comput. Methods Appl. Mech. Engrg.* 79 (1990) 71–86.
- [27] F. Chalot, T.J.R. Hughes, Z. Johan and F. Shakib, Application of the Galerkin/least-squares formulation to the analysis of hypersonic flows: II. Flow past a double ellipse, *Hypersonic Flows for Reentry Problems*, in press.
- [28] F. Shakib, T.J.R. Hughes and Z. Johan, A new finite element formulation for computational fluid dynamics: X. The compressible Euler and Navier–Stokes equations, *Comput. Methods Appl. Mech. Engrg.* 89 (1991) 141–219.
- [29] M.O. Bristeau, M. Mallet, J. Périaux and C. Rogé, Development of finite element methods for compressible Navier–Stokes flow simulations in aerospace design, *AIAA 28th Aerospace Sciences Meeting*, Paper no. 90-0403, Reno, Nevada, 1990.
- [30] R.M. Ferencz, Element-by-element preconditioning techniques for large-scale, vectorized finite element analysis in nonlinear solid and structural mechanics, Ph.D. Thesis, Division of Applied Mechanics, Stanford University, Stanford, CA, 1989.
- [31] J.C. Simo and F. Armero, Geometrically nonlinear enhanced strain mixed methods and the method of incompatible modes, *Internat. J. Numer. Methods Engrg.*, in press.
- [32] J.C. Simo and R.L. Taylor, Quasi-incompressible finite elasticity in principal stretches. Continuum basis and numerical algorithms, *Comput. Methods Appl. Mech. Engrg.* 85 (1991) 273–310.
- [33] T.J.R. Hughes, *The Finite Element Method: Linear Static and Dynamic Finite Element Analysis* (Prentice Hall, Englewood Cliffs, NJ, 1987).
- [34] J.I. Lin, An element eigenvalue theorem and its application for stable time step, *Comput. Methods Appl. Mech. Engrg.* 73 (1989) 283–294.
- [35] D.P. Flanagan and T. Belytschko, A uniform strain hexahedron and quadrilateral with orthogonal hourglass control, *Internat. J. Numer. Methods Engrg.* 17 (1981) 679–706.
- [36] J. Mason, *Functional Analysis for Application in Solid Mechanics* (Elsevier, Amsterdam, 1985).
- [37] V. Girault and P.A. Raviart, *Finite Element Approximation of the Navier–Stokes Equations* (Springer, Berlin, 1979).
- [38] G. Strang and G.J. Fix, *An Analysis of the Finite Element Method* (Prentice Hall, Englewood Cliffs, NJ, 1973).
- [39] L.P. Franca, New mixed finite element methods, Ph.D. Thesis, Division of Applied Mechanics, Stanford University, Stanford, CA, 1987.
- [40] B. Mercier, *Lectures on Topics in Finite Element Solution of Elliptic Problems* (Springer, Heidelberg, 1979).
- [41] D. Givoli and J.B. Keller, A finite element method for large domains, *Comput. Methods Appl. Mech. Engrg.* 76 (1989) 41–66.
- [42] P.G. Ciarlet, *The Finite Element Method for Elliptic Problems* (North-Holland, Amsterdam, 1978).